Science of the Total Environment 968 (2025) 178831

Contents lists available at ScienceDirect

Science of the Total Environment

journal homepage: www.elsevier.com/locate/scitotenv

Combining seepage meters and amphibious electric resistivity tomography to investigate pathways of submarine groundwater discharge

Marc Diego-Feliu[a,b,*], Maria Munoz-Pinyol[c], Jose Tur-Piedra[a,b], Michela Trabucchi[a,b], Aaron Alorda-Kleinglass[c], Raquel González-Fernández[c], Núria Ferrer[a,b], Bella Almillategui[a,b], Audrey Sawyer[d], Carlos René Green-Ruiz[e], Juanjo Ledo[f], Valentí Rodellas[c,g], Albert Folch[a,b]

[a] Department of Civil and Environmental Engineering, Universitat Politècnica de Catalunya (UPC), Barcelona E-08034, Spain
[b] Associated Unit: Hydrogeology Group (UPC), Spain
[c] Departament de Física, Universitat Autònoma de Barcelona, E-08193 Bellaterra, Spain
[d] School of Earth Sciences, The Ohio State University, Columbus 43210, OH, USA
[e] Unidad Académica Mazatlán, Instituto de Ciencias del Mar y Limnología, Universidad Nacional Autónoma de México, Mazatlán 82040, Sinaloa, Mexico
[f] Departamento de Física de la Tierra y Astrofísica, Facultad de Ciencias Físicas, Universidad Complutense de Madrid, Plaza de las Ciencias 1, Madrid 28040, Spain
[g] ICTA, Institut de Ciència i Tecnologia Ambientals, Universitat Autònoma de Barcelona, E-08193 Bellaterra, Spain

HIGHLIGHTS

- Combining geophysics and seepage meters helps identify distinct SGD pathways.
- Nutrient fluxes differ significantly across SGD pathways, even on a local scale.
- Diffuse discharge drives ammonium, while focused discharge dominates nitrate flow.
- A single submarine spring contributes over 50 % of nitrate discharge into the cove.

GRAPHICAL ABSTRACT

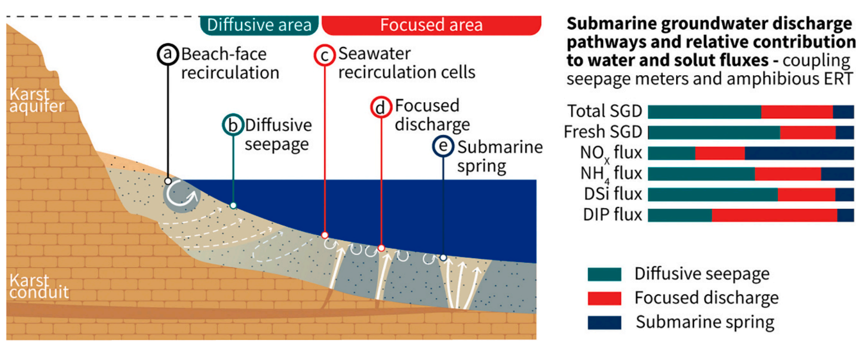

ARTICLE INFO

Editor: Jurgen Mahlknecht

Keywords:
Coastal aquifer
Hydrogeology
Quantification
Geochemistry
Geophysics
Oceanography

ABSTRACT

Submarine groundwater discharge (SGD) plays a pivotal role in coastal biogeochemistry, yet it is still challenging to accurately quantify water and solute fluxes driven by this process due to its complex hydrogeological dynamic. This work aims to improve the methods to identify and independently quantify different pathways of SGD by combining direct measurements through seepage meters and Amphibious Electrical Resistivity Tomography (AERT) at a heterogeneous karstic system in the Mediterranean Sea. The integrated approach identified and quantified distinct SGD pathways, including beach-face recirculation, focused discharge zones, submarine springs, and diffusive discharge, each uniquely influencing SGD dynamics. Given that each pathway is characterized by specific geochemical signatures and discharge rates, nutrient fluxes supplied by different pathways varied significantly in magnitude. In the study site, while diffusive discharge was the primary process for transporting fresh groundwater and ammonium, nitrate and phosphate were mainly delivered to the coastal

* Corresponding author at: Department of Civil and Environmental Engineering, Universitat Politècnica de Catalunya (UPC), Barcelona E-08034, Spain.
E-mail address: marc.diego@upc.edu (M. Diego-Feliu).

https://doi.org/10.1016/j.scitotenv.2025.178831
Received 5 September 2024; Received in revised form 29 January 2025; Accepted 9 February 2025
Available online 21 February 2025

ocean through focused discharge, especially via submarine springs. The combined methodology proved more accurate for determining water and nutrient fluxes than straightforward extrapolations from seepage meters, which were consistently 20 to 120 % higher. This discrepancy highlights the need of combining qualitative and quantitative methods, particularly in regions where multiple SGD pathways coexist.

1. Introduction

Submarine groundwater discharge (SGD) represents an important source of nutrients and contaminants to coastal waters (Moore, 2010; Santos et al., 2021; Wilson et al., 2024) with significant social and environmental implications (Alorda-Kleinglass et al., 2021; Johannes, 1980; Lecher and Mackey, 2018). The process is governed by a set of driving forces (e.g., land-sea hydraulic gradients, density-driven convection, wave and tidal pumping, bioirrigation) from both terrestrial and marine origins (Anwar et al., 2014; Martin et al., 2006; Santos et al., 2012; Schlüter et al., 2000). The driving forces and the groundwater origin (terrestrial or marine), along with the geology and hydraulic parameters of coastal aquifers, determine the temporal and spatial scales of SGD processes (Taniguchi et al., 2002). In turn, these factors ultimately modulate the extent of biogeochemical reactions in the subsurface influencing the concentration of solutes in the discharging groundwater (Goyetche et al., 2022; Spiteri et al., 2008b; Windom and Niencheski, 2003; Wong et al., 2020).

Currently, a wide variety of methods exist to assess SGD qualitatively or quantitatively at various scales (Garcia-Orellana et al., 2021; Taniguchi et al., 2019). Each of the methods captures a specific SGD pathway or a set of them. However, many SGD studies still rely on single-method approaches, which typically provide total SGD estimates and limit the ability to differentiate between fresh and saline SGD or various SGD pathways (Santos et al., 2021). This oversimplification leads to SGD estimates that lack a process-based context, which prevents broader scaling or inter-site comparisons. In contrast, multi-methodological approaches may be instrumental in delineating the magnitude and implications of different SGD pathways (Bejannin et al., 2017; Burnett et al., 2006; Swarzenski et al., 2006a).

Direct assessment methods like seepage meters allow for the direct quantification of groundwater discharge, capturing beach-scale heterogeneities in groundwater flow paths (Duque et al., 2020). Because fluxes can span orders of magnitude over small spatial scales, the accuracy of upscaled flux calculations depends on the number of measurements and their spatial distribution. Accuracy can be improved by using more seepage meters and selecting representative locations based on prior knowledge of the site's hydrogeological characteristics (Duque et al., 2020; Stieglitz et al., 2008; Taniguchi et al., 2007), which is often not available. In these cases, extrapolating point measurements obtained from seepage meters to broader areas may lead to significant biases in the final SGD estimates (Duque et al., 2020). Furthermore, seepage rate measurements are unreliable in strong currents and waves (Cable et al., 2006; Shinn et al., 2002).

Overcoming the limitations of point measurements can be achieved by coupling them with geophysical methodologies that map subsurface properties like salinity, temperature, and resistivity (Paepen et al., 2020; Swarzenski and Izbicki, 2009; Tait et al., 2013; Tur-Piedra et al., 2024). Specifically, geophysical methods have been used along with seepage meters to study groundwater dynamics and the location of the fresh-saltwater interface (Kontar and Ozorovich, 2006; Swarzenski and Izbicki, 2009), to evaluate the spatial and temporal variability of SGD (Durand and Kalyanie, 2014; Stieglitz et al., 2008b; Taniguchi et al., 2006a), to investigate the geochemical cycling of nutrients and trace elements (O'Connor et al., 2015; Sawyer et al., 2014), and to assess SGD flows and its implications (Das et al., 2020; Swarzenski et al., 2007). However, because most geophysical techniques are traditionally designed for use in either terrestrial or marine environments, relatively few studies have addressed the emerged and submerged land-ocean continuum simultaneously (Kroeger et al., 2007; Swarzenski et al., 2006a; Taniguchi et al., 2006b). This area represents a critical transition zone that regulates the magnitude of various SGD pathways, the composition of the discharging groundwater, and the biogeochemical transformations of different compounds before they are discharged (Arévalo-Martínez et al., 2023).

Understanding the land-ocean continuum is particularly important in complex geological settings like karstic aquifers, where flow paths are notoriously heterogeneous and difficult to predict (Beddows et al., 2007; Null et al., 2014; Pain et al., 2019). Karst is present over 15 % of all land (Goldscheider et al., 2020), and 25 % of the world's population lives on karst (Ford and Williams, 2007), yet karst is highly underrepresented in SGD studies (see Fig. 3 of Santos et al. (2021)).

This study aims to advance current approaches for differentiating and quantifying the magnitude of various SGD pathways in highly heterogeneous geologic settings by coupling seepage meter measurements and geochemical analysis with three-dimensional geophysical modeling of the land-ocean continuum. We tested the effectiveness of the proposed method in a karstic system in the microtidal western Mediterranean Sea where groundwater and nutrient discharge have been quantified and compared with an extensive literature review on SGD studies using seepage meters. This study thus advances methods for measuring SGD and offers a conceptual model linking the style of SGD with nutrient loads in karstic settings.

2. Methods

In July 2023, a field campaign was conducted to integrate individual SGD rate measurements from 24 seepage meters with three-dimensional Amphibious Electrical Resistivity Tomography (AERT) data. Additionally, porewater samples were collected along the AERT transects and near each seepage meter for physicochemical and nutrient analysis, aiming to characterize the composition of the discharging groundwater (e.g., Russoniello et al., 2016; Sawyer et al., 2014; W. Brooks et al., 2021). The combination of seepage meters and AERT transects was tested on a sandy beach within a karstic system in the western Mediterranean Sea to assess the significance of different SGD pathways at a local scale.

2.1. Study site

The study site, Aiguadolç Beach, is located in Garraf County, in northeast Spain, along the western Mediterranean Sea (Fig. 1). The beach spans approximately 160 m in length running in an NE-SW orientation and is bordered by fractured and karstified limestone rocky formations at the north and by a block pier at the south (CIIRC, 2010). The main aquifer is the Garraf Jurassic-Cretaceous limestone aquifer, which primarily drives regional groundwater flow in the area. Miocene-Quaternary sediments cover parts of the carbonate aquifer, but these sediments don't constitute a distinct aquifer unit, since its thickness is relatively low and discontinuous. The sediments are composed of conglomerates, sandstones, clays, and marls, and likely influence groundwater flow at the beach scale. Specifically, in the very close coastline, the lithology is composed of fine sand sediments (ca. 90 %; Generalitat de Catalunya, 2010). Originally, the beach consisted of rocky terrain with minimal sand or sediment. Following the construction of the nearby harbor and the urbanization of the Garraf coastline in the mid-20th century, sand was introduced to create a sandy beach. Currently, like several other beaches along this coastline, Aiguadolç

Beach undergoes sediment loss due to storm activity and littoral currents. To address this, local authorities routinely replenish the beach with sediment from nearby dredging sites. The most recent sand replenishment took place in 2017, with approximately 6000 m^3 of sand added (GEM, 2021). Perhaps due to this intervention, the composition of surficial sediments was observed to be quite uniform throughout this relatively small cove. Furthermore, a regional study examining bathymetry, sedimentology, and benthic habitats near our study area (at depths ranging from 8 to 16 m below sea level) found that most sediment samples contained 20–40 % carbonate content and 1–2 % organic matter content (Canals et al., 2021).

The aquifer recharge occurs by direct infiltration of the rainfall and the runoff through a well-developed drainage system. At regional level, the karstification and the tectonic faults and fractures, generate a secondary high permeability and a regional anisotropy (Fig. 1).

Annual average precipitation ranges from 550 mm to 600 mm, with autumn being the rainy season and summer and winter characterized by drier conditions. Winters are moderately cold, with average temperatures between 7 and 9 °C, while summers are warm, averaging 22 to 24 °C. This results in a moderate annual temperature range (SMC, 2023). Waves primarily originate from the South-West and East directions, typically not exceeding a height of 1 m (Puertos del Estado, 2023). Tides in the region follow a semidiurnal regime, with an estimated range of only 0.5 m, typical of the micro-tidal regime of the Mediterranean Sea (CIIRC, 2010).

The specific area under study at Aiguadolç covers a total surface of 4000 m^2. The beach has a gentle slope, with a maximum depth along transects of 1.25 m, located 40 m from the shoreline towards the end of the study area. At the western section of the beach, there is a small ephemeral stream that flows only after extreme precipitation events. The beach is well-known for its freshwater springs, both onshore and submarine (e.g., an onshore spring is in the eastern section of the beach; Fig. 1). These freshwater springs are the reason behind its Catalan name, “Aiguadolç,” which means “fresh water” in English.

2.2. Amphibious electric resistivity tomography

AERT is a geophysical technique designed to assess subsurface resistivity variations encompassing both terrestrial and aquatic environments and allowing for the characterization of the land-ocean transition zone (Kroeger et al., 2007; Swarzenski et al., 2006a; Taniguchi et al., 2006b). The technique provides the combined resistivity of both the solid matrix and the porewater. At the study site, five offshore AERT transects of 60 to 80 m long were established to generate a three-dimensional model illustrating the distribution of resistivity on a beach scale (Fig. 1). The equipment setup featured a 10-channel Iris-Syscal Pro resistivity meter connected to a 12 V battery. To encompass the distinct environments of the emerged and submerged parts of the beach, two different sets of cables and electrodes were employed. Stainless steel electrodes were utilized for the emerged portion of the beach, while a 46-meter multielectrode cable, equipped with 24 graphite electrodes, was employed for the submerged beach. All electrodes were uniformly spaced at 2-m intervals. The deployment of the multielectrode cable across all five transects was conducted manually, with the assistance of a GPS device (Garmin eTrex® 32×) for precise location identification at both ends of each transect. Each electrode was securely buried in the sediment and the cable was anchored with 2 kg lead weights. The elevation of each electrode, relative to the coastline reference level, was measured using an optical level and a telescopic measuring rod, and this data was incorporated into the resistivity transects. Additionally, a roll-along method was used to extend the length of the AERT survey line beyond the initial setup of electrodes, thereby covering a larger area (i.e., a seaward extension of 8 to 12 m in all transects). This extension involved shifting the multielectrode cable seaward after the initial resistivity reading to enhance the reliability of resistivity data for the seaward end. Each data acquisition took approximately 2 h, and all AERT transects were completed over two consecutive days. It is important to note that the sequential acquisition of the AERT transects over two consecutive days introduced potential variability due to sea-level changes. The tidal amplitude during the acquisition period was approximately 8 cm, and these variations may have influenced the distribution of subsurface salinity, thereby affecting the AERT results.

For the 2D inversion of the AERT transects data, the smoothed inversion feature of the *EarthImager* program (Advanced Geosciences) was used. The inversion model assumes homogeneous seabed sediments

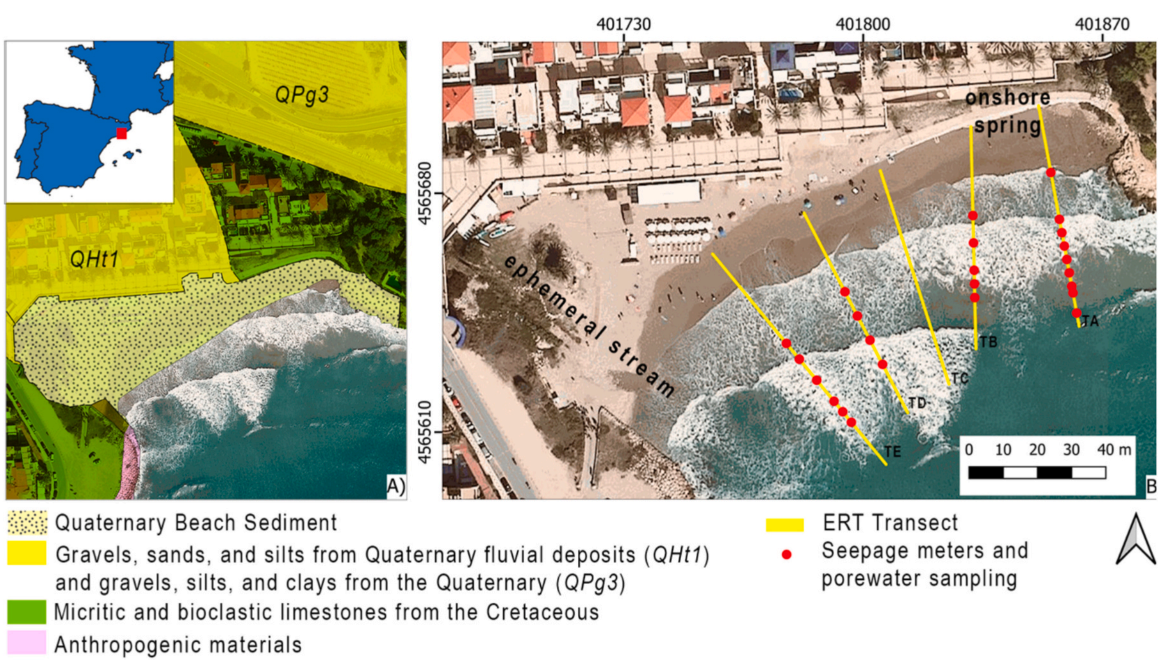

Fig. 1. Study site map. A: Location map of the Aiguadolç beach and geological layout of Aiguadolç Beach. B: Spatial arrangement of seepage meters and porewater sampling, and Amphibious Electrical Resistivity Tomography transects.

with resistivity equal to the average apparent resistivity. The seawater resistivity was set to 0.18 Ω·m, determined based on seawater salinity (see Section 2.3).

The inversion model results from the five AERT transects were used to construct a surface map representing the horizontal spatial variability of the subsurface resistivity. Resistivity data was filtered to include depths ranging from 0.5 to 2 m below the bathymetry level (i.e., ground surface or sediment-water interface), ensuring the focus remains on variations in shallow geological material and porewater. This depth range, was selected to exclude resistivity values from surface seawater and deeper regions (>2 m), allowing comparison with point measurements from seepage meters and manual piezometers (see Section 2.3). Filtered data were used in a geostatistical framework employing the open-source software SGeMS (Remy et al., 2009). The histogram analysis showed a log-normal distribution. Therefore, log-resistivity data were used to define the geostatistical model through the analysis of experimental variograms. The inferred variogram model follows an isotropic exponential function characterized by a range of 22.5 m and a sill of 0.27. The log-resistivity field was ultimately estimated by applying ordinary kriging.

2.3. Discrete measurements: seepage meters, porewater and seawater sampling

2.3.1. Seepage meters

Twenty-four Lee-type manual seepage meters (Lee, 1977) were installed at specific locations to measure SGD rates along 4 shore-perpendicular transects (Fig. 1). The devices consisted of bottomless steel drums with an area of 0.16 m^2 and a height of 20 cm with an outlet on the upper face connected to a 18-mm inner diameter PVC hose attached to a collecting plastic bag (Deltalab™ polypropylene 40 × 75 cm autoclave sterilization bag). The 1-m long PVC hoses were weighted to the seabed to prevent the excessive movement of the plastic bag during water sampling. Seepage meters, hoses, and plastic bags were connected using steel and plastic fittings, previously waterproofed with Teflon tape to avoid water losses. The placement of seepage meters along the transects was based on previous information from preliminary AERT transects to capture the resistivity heterogeneities of the study site. The devices were strategically installed next to AERT electrodes (ca. 0.5 m to the side) in the concurrent survey so that resistivity and discharge measurements could be easily compared. Three to four groundwater discharge rate measurements were done at each seepage meter at the study site during July 2023, representing 78 flux measurements. However, only those samples collected two days after installation are presented to ensure stable geochemical conditions (Murdoch and Kelly, 2003) and mitigate potential measurement errors caused by adverse sea conditions (significant wave height of 0.5–1.0 m; Puertos del Estado, 2024) immediately after installation. It is important to note that, as all seepage measurements were completed within 4 h, the impact of tidal variations on flow measurements is expected to be negligible. The nearest buoy data (offsite) show a total tidal range of approximately 15 cm during the field campaign, typical from a micro-tidal environment, where terrestrial drivers, such as hydraulic gradients, are significantly more influential than the relatively small tidal fluctuations (e.g., Correa et al., 2020; Kreuzburg et al., 2023; Pain et al., 2021). To directly measure recharge and avoid errors due to bag elasticity, seepage bags were prefilled with 500 mL of seawater and then connected to the chambers. Approximately 2 h after installation of the bags, the discharge volume was measured using 1 L and 2 L polypropylene graduated cylinders. Additionally, salinity measurements were conducted on both the initial seawater used to prefill the bags and the recovered water to assess the salinity of the discharging groundwater and determine the fraction of fresh SGD rates relative to the total SGD (Garrison et al., 2003; Martin et al., 2007; Michael et al., 2005).

2.3.2. Porewater and seawater sampling

Porewater sampling was conducted at 54 stations evenly distributed along both the emerged and submerged sections of the AERT transects, adjacent to specific electrodes, enabling comparison of resistivity data with porewater salinity (Fig. 1). Additionally, for nutrient analysis, porewater samples were collected next to each seepage meter for nutrient analysis ($n = 24$). A single seawater sample was collected in the eastern section of the study area, approximately 40 m from the shore, at a depth of 0.5 m below the seawater surface. Porewater sampling was conducted using small and narrow piezometers, consisting of thin stainless-steel tubes with a set of small openings at the end, approximately 3 cm lengthwise, and with an internal diameter of 0.5 cm. The piezometers were inserted into the sediment at a depth of 25 cm, and porewater was extracted using a manual vacuum pump connected to a Büchner flask where porewater was collected. Approximately 300 mL of porewater was collected each time from the piezometers to purge the system, salinity measurements, and nutrient analysis. Collecting this volume ensures the minimization of vertical concentration gradients. Salinity of pore water and seawater were analyzed in the extracted water using a multiparameter probe (YSI Pro Plus).

Samples for the analysis of silicate (SiO_2), phosphate (PO_4^{3-}), nitrite (NO_2^-), nitrate (NO_3^-), and ammonium (NH_4^+) were collected in 10 mL high-density polyethylene (HDPE) vials following filtration through nylon syringe filters with a pore size of 0.45 μm. These vials were promptly placed in a portable refrigerator and subsequently frozen upon arrival at the laboratory for later analysis. The nutrient analysis was conducted using a colorimetric method employing an auto-analyzer (CFA AA3 HR; Seal Analytica) with detection limits of 0.016 μM, 0.010 μM, 0.003 μM, 0.006 μM, and 0.003 μM for SiO_2, PO_4^{3-}, NO_2^-, NO_3^-, and NH_4^+, respectively, a coefficient of variation lower than 0.5 %.

2.4. Quantification of SGD and nutrient fluxes

The fluxes of water and nutrients transported by SGD at beach-scale ($m^3\ d^{-1}$) were calculated using two different approaches. In the first approach, measured seepage rates ($m^3\ m^{-2}\ d^{-1}$) were averaged and then multiplied by the seepage deployment area (ca. 3300 m^2) to estimate the overall water flow. Similarly, for nutrient flux calculations, the seepage rate at each seepage meter was multiplied by the nutrient concentration (mol m^{-3}) from groundwater samples taken nearby. The resulting seepage-derived nutrient flux (mol $m^{-2}\ d^{-1}$) was averaged across all locations and then multiplied by the deployment area to obtain the integrated beach-scale nutrient flux (mol d^{-1}).

The second approach integrated point measurements of seepage rates and nutrient concentrations with the 2-D surface electrical resistivity field. This geophysical and geochemical information, was used to identify distinct SGD pathways, characterized by differences in salinity (inferred from AERT transects), discharge rates, or nutrient composition. A conceptual model of SGD pathways was then developed using this surface map. For each identified SGD pathway, an area of influence was delineated by interpreting the 2D resistivity field. Seepage meters within each pathway's area were used to calculate the average seepage rate specific to that pathway. This method allowed for the assessment of each pathway's contribution to the total beach-scale SGD flows and nutrient fluxes. The total SGD and nutrient fluxes were then calculated as the sum of the individual contributions from all pathways. Throughout the manuscript, seepage rates (Darcy velocities) are reported in cm d^{-1}, as these are the standard units commonly used in most studies employing seepage meters. It is also important to acknowledge that the reported nutrient fluxes may be biased due to the adopted sampling strategy. In contrast to other studies that sampled seepage bags for biogeochemical analysis (e.g., Brooks et al., 2021; Debbie-Ann et al., 2019; Garrison et al., 2003; Leote et al., 2008) to quantify solute fluxes to the coastal ocean, we opted to use nutrient concentrations from single-depth water samples collected near each seepage device at 25 cm below the sediment surface as the endmember for flux calculations. This approach aligns with methodologies employed by many other authors (e.g., Fear et al., 2007; Ibánhez et al., 2011; Szymczycha et al., 2012; Vanek, 1991) and this decision was made taking into account the uncertainties associated with the use of water from the seepage bags; (1) seepage meters can alter redox conditions by restricting oxygen exchange, leading to biogeochemical transformations, (2) they may release compounds like dissolved iron due to corrosion, affecting water composition, and (3) once collected, seepage bag water is exposed to sunlight and temperature changes, further altering its chemistry. These factors can compromise the accuracy of nutrient flux estimates, particularly when comparing seepage meters across different sites. The chosen method (i.e., single-depth porewater sampling) also has inherent uncertainties, which we acknowledge. This approach does not account for potential biogeochemical transformations that may occur over the short distance between the sampling depth and the actual discharge point, introducing some uncertainty in the calculated fluxes. Such limitations have been extensively highlighted in previous studies (e.g., Sawyer et al., 2014; Weinstein et al., 2011; Wong et al., 2020) and represent a common challenge in SGD research, as frequently discussed in the literature (e.g., Cerdà-Domènech et al., 2017; Cho and Kim, 2016; Rodellas et al., 2021; Santos et al., 2021).

The relative contributions of fresh and recirculated SGD at each seepage meter were determined by first calculating the salinity of the discharging groundwater (C_{SPG}). This calculation was based on the initial and final salinity measurements (C_0 and C_f, respectively) and the initial and final volumes in the seepage bag (V_0 and V_f, respectively, in m^3) (Eq. (1)). The final volume, V_f, is given by $V_f = V_0 + V_{SPG}$, where V_{SPG} is the volume of groundwater seeping during the sampling period.

$$C_{SPG} = C_f + \frac{V_0}{V_{SPG}}\left(C_f - C_0\right), \tag{1}$$

then the fresh and recirculated seepage rate (Q_F and Q_R, respectively in $m^3\ m^{-2}\ d^{-1}$), were calculated using water and salinity mass balances;

$$\begin{aligned} Q_{SPG} &= Q_F + Q_R \\ Q_{SPG}C_{SPG} &= Q_F C_F + Q_R C_R \end{aligned}, \tag{2}$$

where Q_{SPG} is the discharge rate of each seepage ($m^3\ m^{-2}\ d^{-1}$) and C_F and C_R are the salinities of fresh and saline endmembers, respectively. The selection of endmembers was done by using the freshest groundwater salinity of all porewater samples for C_F and seawater salinity for C_R.

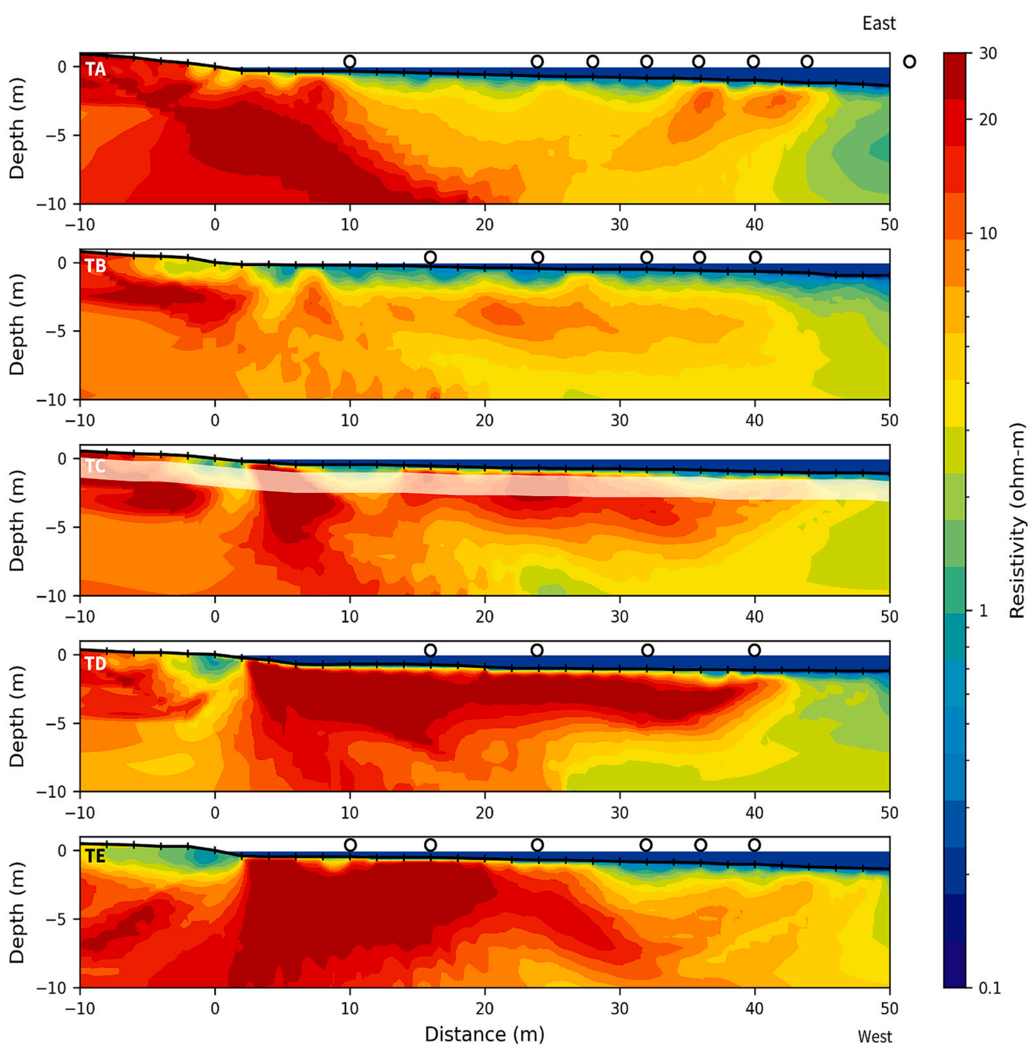

Fig. 2. Shore-perpendicular AERT transects conducted during the sampling of July 2023 from east (TA) to west (TE) direction in Aiguadolç beach. The 0-distance value represents the shoreline, and negative and positive values represent the terrestrial and marine parts of the AERT transect, respectively. Circles represent the locations where seepage meters were installed. The resistivity range displayed is limited to 30 Ω·m in the upper range to ensure clear visualization of the relevant resistivity changes and the semi-transparent white band in TC represents the depths used for 2-D surface map interpolation.

3. Results

3.1. Subsurface resistivity

Subsurface resistivity at the study site, determined from AERT transects, ranges from 0.01 to 180 Ω·m. Lower resistivity values (0.01 to 2 Ω·m) are typically indicative of sediment saturated with seawater, while higher resistivity values (>2 Ω·m) suggest the presence of fresh or brackish groundwater (Day-Lewis et al., 2006; Paepen et al., 2020). Therefore, the resistivity data from the AERT transects at the study site likely indicate a mix of fresh and saline groundwater (Fig. 2). It is important to note that variations in resistivity may not solely reflect changes in porewater salinity but could also result from variations in sediment composition. Nevertheless, the surficial sediments were qualitatively consistent in texture where we installed electrodes. A discernible trend is observed across all transects, characterized by elevated resistivity values at the inland region of the transect, progressively decreasing in the seaward direction. Minimum resistivity values are found at the seaward end of the transects. The 2-D surface map of interpolated resistivity (Fig. 4) reveals a low-resistivity area extending horizontally from the surf zone landward, ranging from 2 to 10 m, depending on the AERT transect. This low-resistivity region is more extensive in the eastern transects compared to the western transects. In the eastern segment of the beach, high-resistivity zones are unevenly distributed and frequently overlain by regions of lower resistivity. A notable high-resistivity area, approximately 100 m^2 in size, is observed in the eastern most seaward part of the surface map (Fig. 4). Conversely, the western part of the beach is predominantly characterized by a large and relatively homogeneous high-resistivity zone (Fig. 4). Resistivity at 0.5 to 2 m depth not strongly correlated with porewater salinity along the AERT transects (Supplementary Fig. S1), likely due to three factors: 1) complexity in vertical resistivity structure and its relationship to three-dimensional flow paths across the sediment-water interface, 2) the different support volumes of resistivity at pixels (which are inverted rather than directly measured) and porewater salinities, which are localized to small volumes (Ward et al., 2010; Zhang et al., 2023), and 3) the influence of the solid matrix on bulk resistivity (which we believe to be relatively minor at this site). However, higher salinities (above 15) generally correspond to lower resistivities (below 20 Ω·m), while lower salinities are linked to higher resistivity values (Supplementary Fig. S1).

3.2. Seepage meter discharge rates

The seepage flow rates ranged from -0.2 ± 0.1 to 86.3 ± 4.3 cm d^{-1} with a mean discharge rate of 25.7 cm d^{-1} (see Table S1 for more details). These rates are consistent with seepage rates reported in studies worldwide, as shown in the literature review (Fig. 3). The relative discharge rate of fresh groundwater ranged from 0 % to 94 % of the total discharge (mean of 46 %) (Fig. 4), with mean seepage rates of 16.8 cm d^{-1} for fresh groundwater and 9.0 cm d^{-1} for recirculated groundwater.

The spatial distribution of seepage rates showed substantial heterogeneity along the beach. Recirculated SGD exhibited relatively constant values, differing by less than one order of magnitude (interquartile range (IQR): 4.0–13.5 cm d^{-1}). In contrast, fresh groundwater discharge varied significantly, with almost two orders of magnitude of difference (IQR: 0.7–30.0 cm d^{-1}). Generally, lower seepage rates were observed in seepage meters located nearest to the coast, particularly in low-resistivity areas (Fig. 4). Conversely, higher seepage rates were found in the most seaward portions of the AERT transects, with a peak fresh groundwater discharge of 70.7 ± 4.4 cm d^{-1}, occurring 40 to 50 m from the shore in the eastern transect (TA in Fig. 2). The maximum seepage rates reported here are comparable with those reported in other studies with similar geological settings (e.g., 190 cm d^{-1}, Leote et al., 2008; 40 cm d^{-1}, Montiel et al., 2018; 370 cm d^{-1}, Povinec et al., 2012; 180 cm d^{-1}, Prakash et al., 2018; 40 cm d^{-1}, Rapaglia, 2005; 70–360 cm d^{-1}, T. Stieglitz et al., 2008a; 90 cm d^{-1}, Taniguchi et al., 2008a). However, no correlation is observed between water flows (fresh, saline, or total) and resistivity (see Fig. S1). This lack of correlation is not unexpected, as groundwater composition (e.g., salinity inferred from resistivity variations) does not directly indicate the magnitude of SGD flow. Rather, the magnitude of SGD pathways is influenced by their driving force (e.g., hydraulic gradients, density-driven flow, bioturbation), which can lead to the discharge of both fresh and saline groundwater in varying proportions depending on the specific characteristics of the study site (e.g., Pain et al., 2021; Santos et al., 2012; Taniguchi et al., 2019).

3.3. Nutrient concentrations

Nutrient concentrations in groundwater samples at the study site ranged from 0.06 to 1.00 μmol·L^{-1} for phosphate, from 18 to 52 μmol·L^{-1} for silicate, from 0.02 to 0.84 μmol·L^{-1} for nitrite, from 1.4 to 230 μmol·L^{-1} for nitrate, and from 85 to 410 μmol·L^{-1} for ammonium (Fig. 5). The dissolved inorganic phosphorus (DIP) and dissolved inorganic nitrogen (DIN) concentrations in this study were comparable with other Mediterranean karstic areas (Alorda-Kleinglass et al., 2024; Chen et al., 2020; Garcia-Solsona et al., 2010; Tamborski et al., 2020; Tovar-Sánchez et al., 2014). The inorganic nitrogen speciation is dominated by ammonium (median: 180 μM; IQR: 130–270 μM), with concentrations generally 1 to 2 orders of magnitude higher than nitrate (median: 5.9 μM; IQR: 4.1–9.3 μM) and 4 orders of magnitude higher than nitrite concentrations (median: 0.04 μM; IQR: 0.02–0.09 μM), as commonly observed in coastal porewaters (Devol, 2015; Rigaud et al., 2013; Rodellas et al., 2018). The seawater sample collected at the eastern part of the beach exhibited relatively high DIP, dissolved silica (DSi), and DIN concentrations of 0.04, 3.1, and 180 μM, respectively. It is noteworthy that all groundwater samples displayed high DIN:DIP ratios (from 100:1–6000:1) exceeding the Redfield ratio of 16:1, which could exacerbate phosphorus limitation in the coastal ocean. This situation is particularly prevalent in the Mediterranean Sea and other regions globally (Chen et al., 2020; Rodellas et al., 2015; Santos et al., 2021).

4. Discussion

4.1. SGD pathways

Identifying and distinguishing different SGD pathways is fundamental to accurately constrain both the discharge of water and solutes to the coastal ocean. The geophysical information and seepage rates in Aiguadolç Beach indicate the presence of at least 5 different SGD pathways (Fig. 6). At the shoreline, (1) beach-face recirculation of seawater induced by waves generates seawater circulation cells of 5 to 10 m in length in the shore-perpendicular direction and 2 m in depth as inferred by the AERT transects (Figs. 2 and 4). At the eastern region of the beach (2) focused discharge of groundwater occurs both at the coastline and offshore. The localized nature of the discharge might be associated with the presence of karstic conduits and fractures of the bedrock, as it is expected based on historical information suggesting that the beach sediment thickness is relatively thin, as limestone rock was outcropping just a few decades ago. If the magnitude of the discharge and the affected area is relatively significant, these karstic features can develop into (3) submarine springs, as such observed between 35 and 45 m along the eastern transect (TA; Fig. 2), where the highest seepage rates in the area have been recorded (Fig. 4). These focused discharge areas are surrounded by the presence of saltier groundwater which may generate (4) density-driven recirculation cells of 4 to 6 m in length with relatively low discharge. Finally, at the western section of the beach, geophysical data show the presence of a large and continuous (25 to 40 m length) high resistivity body indicating (5) diffusive discharge of groundwater which might be a mixture of meteoric groundwater and recirculated seawater (Fig. 4). The diffuse nature of SGD in this area may stem from the absence of karst conduits in the bedrock, unlike those in the eastern section of the cove, or it may be linked to a thicker alluvial

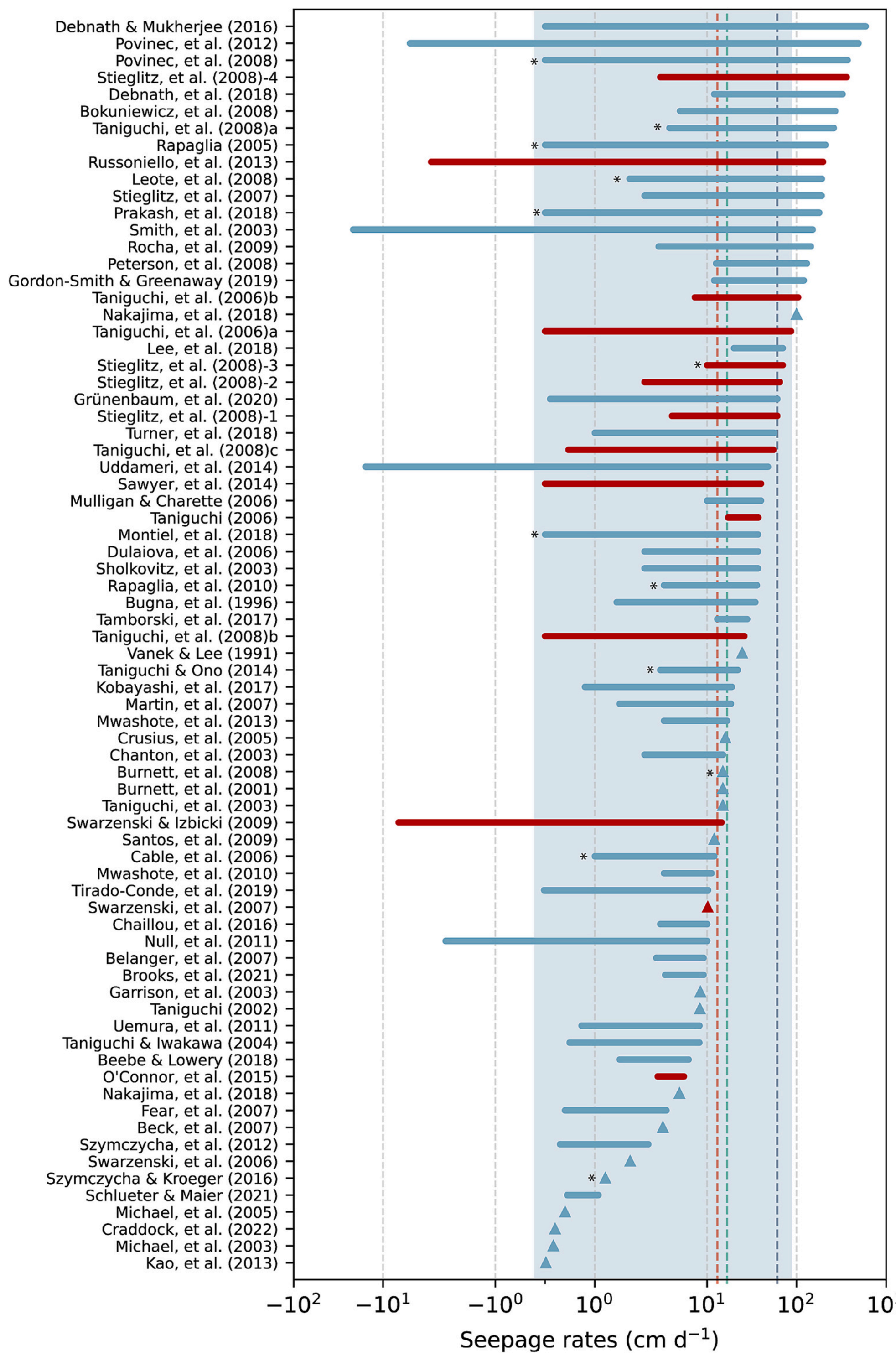

Fig. 3. Seepage rates as reported by various authors, with values presented in ranges of minimum and maximum values represented by lines. In instances where specific ranges are not provided, averages are denoted by triangles. Red lines or triangles represent articles that have concurrently employed seepage meters and geophysical data, and asterisks those in karstic systems. The vertical blue band is the range value of the data presented in this manuscript, and red, green, and blue dashed lines are the mean value of focused, diffusive, and submarine spring areas, respectively. The comprehensive literature review encompassed a total of 110 articles, from which seepage rates were reported in only 74 cases, and the combined use of seepage meters and geophysical methods in 14 cases (Beck et al., 2007; Beebe and Lowery, 2018; Belanger et al., 2007; Bokuniewicz et al., 2008; Bugna et al., 1996; Burnett et al., 2001; Burnett et al., 2008; Chaillou et al., 2016; Chanton et al., 2003; Craddock et al., 2022; Crusius et al., 2005; Debnath and Mukherjee, 2016; Gordon-Smith and Greenaway, 2019; Debnath et al., 2018; Lee et al., 2018; Mulligan and Charette, 2006; Dulaiova et al., 2006; Grünenbaum et al., 2020; Kao et al., 2013; Kobayashi et al., 2017; Michael et al., 2003; Mwashote et al., 2010; Mwashote et al., 2013; Nakajima et al., 2018; Null et al., 2011; Peterson et al., 2008; Povinec et al., 2008; Rocha et al., 2009; Rapaglia et al., 2010; Russoniello et al., 2013; Santos et al., 2009; Schlueter and Maier, 2021; Sholkovitz et al., 2003; Smith et al., 2003; Stieglitz et al., 2007; Swarzenski et al., 2006b; Szymczycha et al., 2016; Tamborski et al., 2017; Taniguchi, 2002; Taniguchi, 2006; Taniguchi and Iwakawa, 2004; Taniguchi et al., 2008b, 2008c, 2014; Tirado-Conde et al., 2019; Turner et al., 2018; Uddameri et al., 2014; Uemura et al., 2011; Vanek and Lee, 1991).

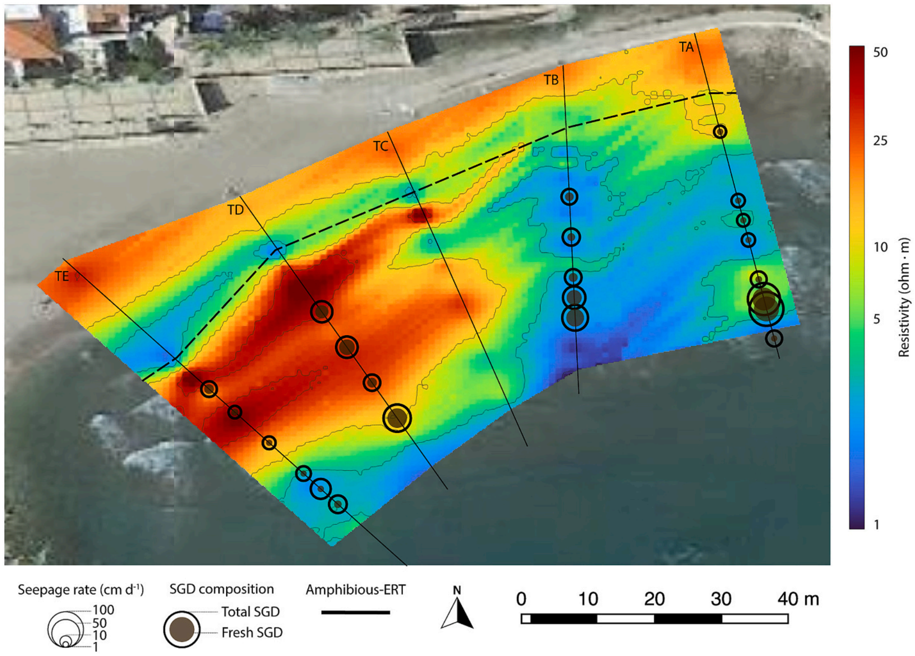

Fig. 4. Total and fresh SGD as measured using seepage meters along AERT shore-perpendicular transects at Aiguadolç Beach and resistivity depth-slice from the AERT survey (integrating data between 0.5 and 2 m depths). The size of the transparent and gray circles represents the magnitude of the measured seepage rate for total and fresh SGD, respectively. Dashed line represents the coastline.

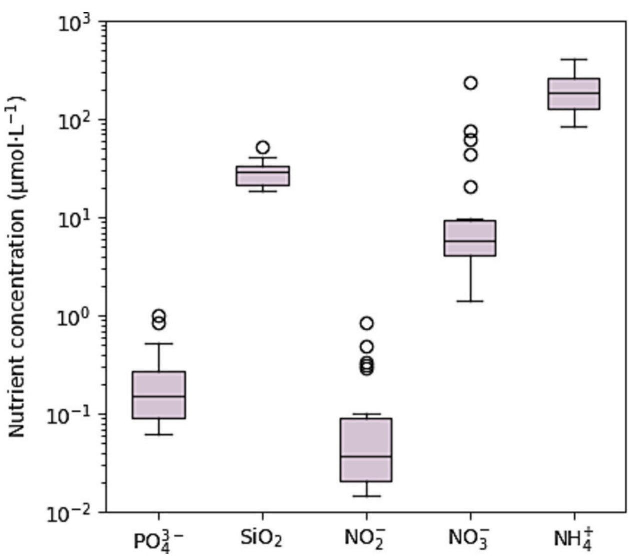

Fig. 5. Phosphate (PO_4^{3-}), silicate (SiO_2), nitrite (NO_2^-), nitrate (NO_3^-), and ammonium (NH_4^+) concentrations in groundwater samples collected in the vicinity of the deployed seepage meters.

deposit on the western side of the beach, which was likely transported by the ephemeral stream.

4.2. Coupling AERT and seepage meters for quantifying SGD

The combination of AERT and seepage meters enables the quantification of individual SGD pathways based on the zonation and the observed seepage rates. Three distinct areas have been identified based on the conceptual discharge model (Fig. 6): the beach-face recirculation area, the diffusive area, and the focused area (Fig. 7). Notably, the focused area encompasses various pathways, as it can be inferred from the variability in the total and fresh discharge rate. These pathways may include focused discharge, density-driven recirculation cells, and the submarine spring. However, the submarine spring has been independently quantified due to its unique characteristics. At the beach-face recirculation area, no seepage meters could be deployed due to the low water column depth. However, resistivity data (1–5 Ω m) and porewater salinity (20–36) indicate the discharge of recirculated seawater with a significant contribution of meteoric groundwater. Seepage meters located at the diffusive discharge area had relatively high seepage rates (mean and standard error of the mean; 25 ± 8 cm d^{-1}; $N = 7$) with a high contribution of fresh groundwater discharge (70 %), relative to total SGD. This is consistent with the large high-resistivity body present in this area and extending across AERT transects TC, TD, and TE (Fig. 4). Conversely, seepage rates at the focused discharge area (excluding the submarine spring), which is dominated by the presence of localized discharge tubes and saline recirculation cells, were relatively low (18 ± 5 cm d^{-1}; $N = 10$), and mostly associated with the discharge of saltier groundwater (relative contribution of fresh seepage of 30 %). Notably, the submarine spring in this region exhibited the highest seepage rates in the cove, averaging 60 ± 23 cm d^{-1} ($N = 3$), with fresh groundwater constituting 60 % of the discharge (Fig. 7).

By combining the areas of influence of each SGD pathway and their mean measured seepage rates (Fig. 7), it can be established that diffusive seepage was the main SGD pathway at Aiguadolç Beach. It contributed 56 % of the total SGD (420 ± 140 m^3 d^{-1}) and 64 % of the fresh SGD (340 ± 120 m^3 d^{-1}) in the cove (Fig. 8). In contrast, focused discharge accounted for 35 % of the total discharge (260 ± 82 m^3 d^{-1}) and 27 % of the fresh groundwater discharge (140 ± 70 m^3 d^{-1}). Despite its small area of influence, the single submarine spring in the eastern region of the cove (Fig. 7) was responsible for 8 % of the total SGD and 9 % of the fresh SGD at the site, with rates of 60 ± 20 and 50 ± 20 m^3 d^{-1}, respectively. Compared to other submarine springs along the Mediterranean coastline, our results are substantially lower (e.g., 0.8–1.6 • 10^6 m^3 d^{-1}, Garcia-Solsona et al., 2010; 2.1 • 10^5 m^3 d^{-1}, Mejías et al., 2012; 0.2–1.1 • 10^5 m^3 d^{-1}, Pavlidou et al., 2014). These differences may reflect the presence of an overlying sediment layer in our study area, which could attenuate discharge flow, as well as the absence of large ephemeral streams that significantly enhance SGD in other regions.

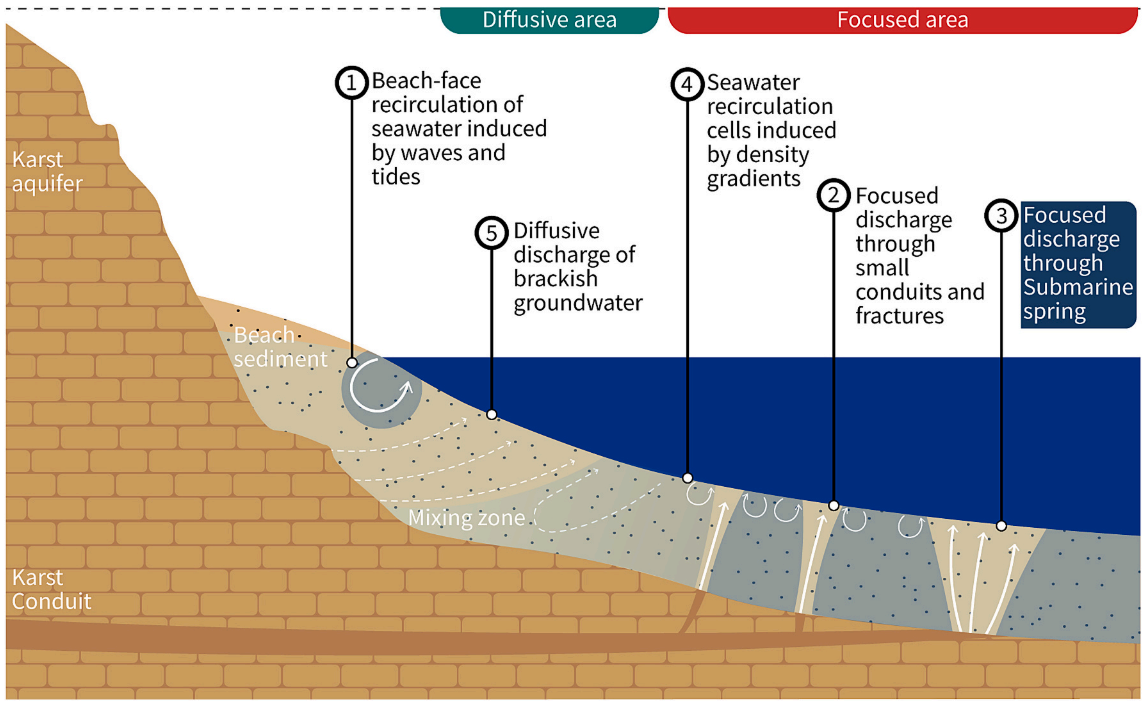

Fig. 6. Conceptual diagram of SGD pathways in Aiguadolç Cove. The pathways are grouped and categorized into diffuse areas, focused areas, and submarine springs. Each of these pathways is independently quantified in Sections 4.2 and 4.3.

The relatively low contribution of focused discharge to the total SGD at Aiguadolç, particularly in terms of fresh SGD, might be associated with the heterogeneity of the area, which encompasses multiple discharge pathways, and the biases related to the placement of seepage meters (Duque et al., 2020; Murdoch and Kelly, 2003; Taniguchi et al., 2003). It is important to note that, unlike the diffusive seepage area where discharge flows are relatively consistent, focused SGD is highly localized. Accurate measurement in such areas requires high spatial resolution sampling and precise positioning of seepage meters to ensure coverage of various discharge processes (Burnett et al., 2006). Contrastingly, the results of combining seepage meters with AERT are instrumental in identifying and quantifying relatively large submarine springs such as the one located in the eastern region of the cove (Fig. 7).

The results showed that the integration of AERT and seepage meters has proven instrumental in unraveling the small-scale dynamics of SGD within a karst area with highly heterogeneous geology and flow rates. This combined approach enabled the creation of a conceptual model of SGD at the study site, including the identification of five distinct SGD pathways, each involving the discharge of groundwater with varying compositions.

4.3. Implications for SGD estimates

Accurate SGD estimates are fundamental for assessing the environmental and social relevance of this process worldwide (e.g., Alorda-Kleinglass et al., 2021; Lecher and Mackey, 2018; Moosdorf and Oehler, 2017) and capturing the potential effect of climate change and induced meteorological and oceanographic events on the magnitude of SGD fluxes (e.g., Adyasari et al., 2021; Diego-Feliu et al., 2022; Richardson et al., 2024). The accuracy of the estimates requires adequately gauging the magnitude of water flows and transforming this volumetric discharge to solute fluxes. However, this is especially challenging in heterogeneous systems, particularly karstic areas, such as Aiguadolç Beach, with the presence of multiple concurrent SGD pathways (Burnett et al., 2003).

Concerning the quantification of water flows, the integration of seepage meters and AERT has facilitated the differentiation of various SGD pathways illustrating their distribution along the beach area. However, concerning the quantification of the overall discharge into the cove (derived from individual SGD pathways estimates, Section 4.2), the estimates do not significantly deviate from those obtained by simply extrapolating individual seepage rates through a straightforward averaging approach, showing disparities of approximately 22 % and 15 % for total and fresh SGD, respectively (Fig. 8). Nonetheless, the benefit of individually quantifying distinct SGD pathways lies in the improved understanding of solute fluxes, given that each pathway is expected to exhibit a unique chemical signature (e.g., Slomp and Van Cappellen, 2004; Spiteri et al., 2008b, 2008a).

This is the case for Aiguadolç Beach where groundwater nutrient enrichment varies among SGD pathways (Fig. 8). Samples from diffusive area exhibited lower variability, displaying narrower ranges of DIP (0.06–0.21 μM), DSi (19–32 μM), and DIN (120–230 μM) relative to those in the focused discharge area (DIP: 0.07–1.00 μM; DSi: 19–52 μM; DIN: 90–380 μM) which exhibited greater dispersion due to the heterogeneity of the area and the variety of discharge processes. Notably, the samples collected at the submarine spring exhibited the highest concentrations of DIN, ranging from 460 to 530 μM. In all groundwater samples, ammonium was the predominant species of inorganic nitrogen. This was especially pronounced in samples from the diffusive area, where ammonium constituted >90 % of the total DIN. In contrast, the submarine spring samples had lower NH_4:DIN ratios relative to the diffusive area (with ammonium comprising 50 % to 90 % of the total DIN), indicating a higher proportion of nitrate in this area.

Both, the higher DIN concentrations, and the relatively higher proportions of nitrate in samples collected at the submarine spring may be indicative of higher groundwater velocities which may hinder the removal processes of inorganic nitrogen (e.g., denitrification, anaerobic oxidation of ammonium, adsorption into sediment surface; Bernard et al., 2014; Jiao et al., 2018; Wu et al., 2021) and the reduction of nitrate to ammonium mediated by microbial communities (Dissimilatory Nitrate Reduction to Ammonia; Bernard et al., 2015; Brooks et al., 2021). These processes may take place in the diffusive area due to the lower velocities of groundwater, which increases the reaction time between solutes and aquifer solids (Devol, 2015). Furthermore, the higher

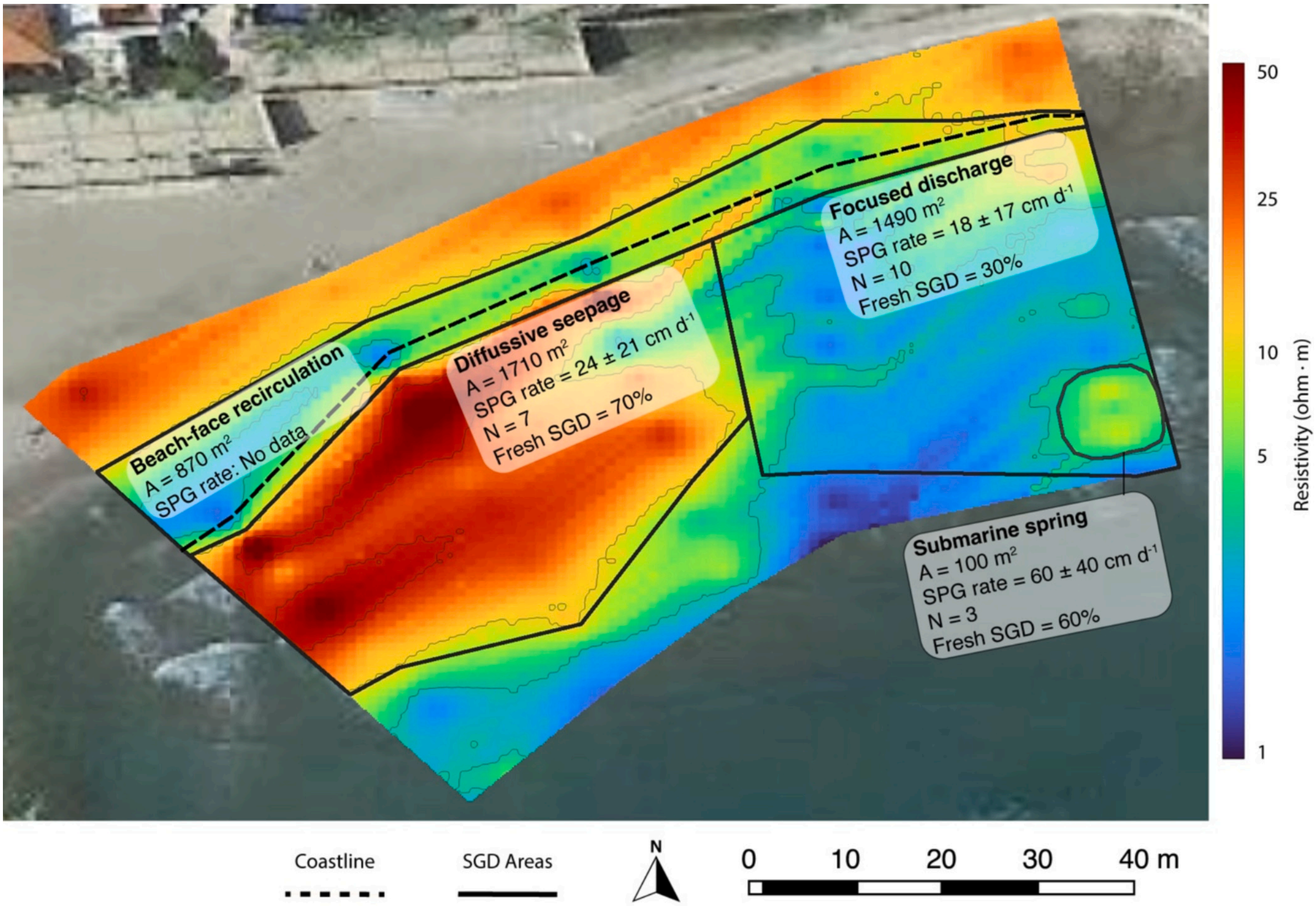

Fig. 7. Area (A), seepage rate (SPG rate), number of seepage meters (N), and relative proportion of fresh SGD in percentage (Fresh SGD) of the different SGD pathways in Aiguadolç Beach and AERT surface (0.5 to 2 m depths) interpolation. Black lines represent the border of the different discharge areas and dashed line represent the coastline.

concentrations of phosphate in the focused area compared to the diffusive area may suggest that seawater recirculation drives the degradation of organic matter, releasing phosphate into the water column. In contrast, phosphorus attenuation in the diffusive area could be attributed to coprecipitation and adsorption into the solid matrix (Robinson et al., 2018; Spiteri et al., 2008a). The behavior of phosphorus is highly complex and may be influenced by the redox conditions of the porewater, as well as the presence and specific cycling of manganese and iron oxides within the subterranean estuary (Gonneea and Charette, 2014; Roy et al., 2013, 2012). Understanding nutrient transformations along groundwater flow paths is inherently complex and requires comprehensive biogeochemical sampling, which falls beyond the scope of this manuscript.

The geochemical signatures of each pathway led to significant differences in the SGD-derived nutrient flux. The submarine spring DIP, DSi, and DIN fluxes (0.11, 17, and 290 mmol m^{-2} d^{-1}, respectively) were the highest in comparison with fluxes of the diffusive seepage (0.03, 7, and 50 mmol m^{-2} d^{-1}, respectively), the focused area (0.06, 3, and 30 mmol m^{-2} d^{-1}, respectively) and within the range of the reported nutrient fluxes worldwide (Santos et al., 2021). The area-normalized flux considering the influence area of each SGD pathway as inferred by AERT profiles at the cove of Aiguadolç was 0.1 mol·d^{-1} for DIP, 20 mol·d^{-1} for DSi, and 110 mol·d^{-1} for DIN. However, the relative significance of each SGD pathway varied depending on the kind of nutrient considered; while diffusive seepage was the primary pathway transporting groundwater, ammonium, and silicate to the coastal ocean, discharge through the focused discharge area was the main pathway for nitrate and phosphorus, with the submarine spring accounting for over 50 % of the total nitrate discharge (Fig. 8). The quantification of overall nutrient fluxes by integrating AERT data and seepage meters and distinguishing SGD pathways varies significantly relative to the straightforward averaging method. The average method tends to overestimate the overall water flows by a factor of 2 for nitrate, ammonium, and phosphorous (Fig. 8).

These findings highlight the importance of separately examining SGD pathways and their influence on coastal biogeochemistry. Relying solely on point-measurement estimates, a common approach using seepage meters (Fig. 3), to determine total SGD can introduce significant deviations and biases in both groundwater flow and associated solute fluxes. Despite this, the integration of quantitative data from seepage meters with prospective techniques like resistivity profiling remains relatively scarce in the literature. Only 14 studies have reported concurrent use of seepage meters and geophysical techniques, and of these, only one was conducted in a karstic system (Fig. 3). Furthermore, most articles using ERT techniques have focused on either marine or terrestrial environments, with only a few examples employing amphibious techniques (AERT) that encompass both environments (Kroeger et al., 2007; Swarzenski et al., 2006a; Taniguchi et al., 2006b).

5. Conclusions

The combination of Amphibious Electric Resistivity Tomography (AERT) and seepage meters has provided valuable insights into the complex dynamics of Submarine Groundwater Discharge (SGD)

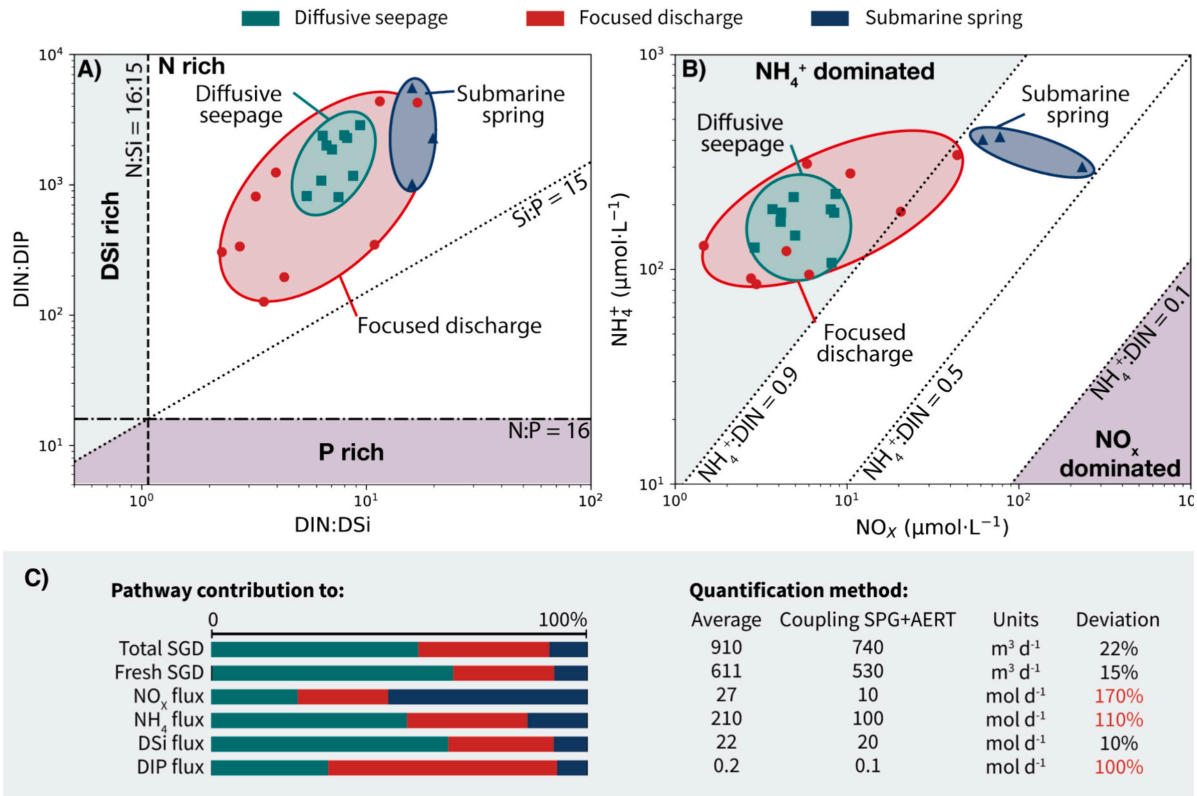

Fig. 8. Nutrient limitation (A) and dissolved inorganic nitrogen (DIN) speciation (B) of the groundwater samples collected in the vicinity of the seepage meters. Red circles, green squares, and blue triangles represent the samples collected in the focused discharge, diffusive seepage, and submarine spring areas, respectively. C) Summary of SGD pathway contribution to total water flows and nutrient fluxes at the study site and comparison between quantification methods.

pathways and their implications for coastal biogeochemistry in a highly heterogeneous karstic beach of the Mediterranean Sea. High-resolution 3D resistivity data revealed distinct SGD pathways, including beach-face recirculation, focused discharge, submarine springs, density-driven recirculation cells, and diffusive discharge. Each of these pathways contributes uniquely to the overall SGD dynamics at the study site. The study emphasizes the importance of independently quantifying distinct SGD pathways and their area of influence to accurately determine solute fluxes to the coastal ocean, rather than expressing estimates as total SGD. It was found that while diffusive discharge was the primary pathway for SGD and ammonium, focused discharge—particularly through a submarine spring—was the main process for nitrate and phosphate delivery to the coastal ocean. Because focused submarine springs make an important contribution to fluid and geochemical fluxes and are difficult to predict in terms of number and location, integrated AERT and seepage meter studies can substantially improve the accuracy of water and nutrient fluxes estimates, reducing the conceptual uncertainties. The methodological setup presented here is instrumental not only for understanding groundwater and solute fluxes but also for assessing biogeochemical transformations across the land-ocean continuum. Additionally, it can be used for monitoring coastal groundwater dynamics, whether seasonal or associated with episodic events. This study underscores the necessity of combining qualitative and quantitative measurements to obtain more reliable and accurate estimates of submarine groundwater discharge (SGD). Such an approach is essential for improving our comprehension of groundwater discharge mechanisms in heterogeneous coastal settings such ad karst systems.

CRediT authorship contribution statement

Marc Diego-Feliu: Writing – review & editing, Writing – original draft, Visualization, Validation, Methodology, Investigation, Formal analysis, Data curation, Conceptualization. **Maria Muñoz-Pinyol:** Writing – original draft, Visualization, Validation, Methodology, Investigation, Formal analysis, Data curation, Conceptualization. **Jose Tur-Piedra:** Writing – review & editing, Visualization, Validation, Methodology, Investigation, Formal analysis, Data curation, Conceptualization. **Michela Trabucchi:** Writing – review & editing, Writing – original draft, Visualization, Validation, Methodology, Investigation, Formal analysis, Data curation. **Aaron Alorda-Kleinglass:** Writing – review & editing, Validation, Methodology, Investigation, Conceptualization. **Raquel González-Fernández:** Writing – original draft, Methodology, Investigation, Formal analysis, Data curation, Conceptualization. **Núria Ferrer:** Writing – review & editing, Writing – original draft, Investigation. **Bella Almillategui:** Writing – review & editing, Methodology, Data curation. **Audrey Sawyer:** Writing – review & editing, Investigation. **Carlos René Green-Ruiz:** Writing – review & editing, Methodology, Investigation, Data curation. **Juanjo Ledo:** Writing – review & editing, Supervision, Resources, Methodology, Investigation, Formal analysis, Data curation, Conceptualization. **Valentí Rodellas:** Writing – review & editing, Resources, Project administration, Methodology, Investigation, Funding acquisition, Conceptualization. **Albert Folch:** Writing – review & editing, Supervision, Resources, Project administration, Methodology, Investigation, Funding acquisition, Conceptualization.

Funding sources

This research has been supported by the Catalan Water Agency (grant no. ACA210/18/00007), the projects PID2022-140862OB-C21 and PID2022-140862OB-C22 funded by MCIN/AEI/10.13039/501100011033/ and "FEDER Una manera de hacer Europa", and the fundings from the Direcció General de Recerca from Generalitat de Catalunya (grant: 2021-SGR 00609). M.D-F acknowledges financial support from grant JDC2022-050316-I funded by MCIN/AEI/10.13039/501100011033 and by the European Union - NextGenerationEU/PRTR. J.T-P acknowledges the economic support from the FI-2022 fellowships of the Generalitat de Catalunya autonomous government (2022FI_B_00601). C.G-R thanks the sabbatical fellowship awarded by PASPA-DGAPA from Universidad Nacional Autónoma de México. B.A is supported with a Doctoral Research Scholarship (BIDP-I-2020-016) awarded by SENACYT-IFARHU from the Republic of Panama.

Declaration of competing interest

The authors declare that they have no known competing financial interests or personal relationships that could have appeared to influence the work reported in this paper.

Acknowledgments

This work is dedicated to Jordi Garcia Orellana, a devoted professor, mentor, and friend whose passion and dedication inspired and encouraged many throughout his career. The authors would like to thank all colleagues from the Grup de Recerca en Radioactivitat Ambiental de Barcelona – GRAB (Universitat Autònoma de Barcelona), the Grup d'Hidrologia Subterrània - GHS (Universitat Politècnica de Catalunya), the students from the Environmental Sciences degree of the Universitat Autònoma de Barcelona (UAB) for participating in the sampling campaigns and the EXES group from the Universitat de Barcelona for their support with AERT equipment and scientific help. The authors would also like to acknowledge the contributions of Rafael Moraira Reina, Jordi López Santos, Ernesto Asensio Sosa, and Albert Gargallo Garriga from the Technical Physics Services at UAB for their work in constructing the seepage meters, the Sitges City Council for allowing us to work at Aiguadolç Beach and for providing us with storage spaces, and Maravillas Abad from ICM-CSIC for the analysis of nutrients.

Appendix A. Supplementary data

Supplementary data to this article can be found online at https://doi.org/10.1016/j.scitotenv.2025.178831.

Data availability

Data will be made available on request.

References

Adyasari, D., Montiel, D., Mortazavi, B., Dimova, N., 2021. Storm-driven fresh submarine groundwater discharge and nutrient fluxes from a barrier island. Front. Mar. Sci. 8, 1–17. https://doi.org/10.3389/fmars.2021.679010.

Alorda-Kleinglass, A., Ruiz-Mallén, I., Diego-Feliu, M., Rodellas, V., Bruach-Menchén, J. M., Garcia-Orellana, J., 2021. The social implications of submarine groundwater discharge from an ecosystem services perspective: a systematic review. Earth Sci Rev 221, 103742. https://doi.org/10.1016/j.earscirev.2021.103742.

Alorda-Kleinglass, A., Rodellas, V., Diego-Feliu, M., Marbà, N., Morell, C., Garcia-Orellana, J., 2024. The connection between submarine groundwater discharge and seawater quality: the threat of treated wastewater injected into coastal aquifers. Sci. Total Environ. 922, 170940. https://doi.org/10.1016/j.scitotenv.2024.170940.

Anwar, N., Robinson, C.E., Barry, D.A., 2014. Influence of tides and waves on the fate of nutrients in a nearshore aquifer: numerical simulations. Adv. Water Resour. 73, 203–213. https://doi.org/10.1016/j.advwatres.2014.08.015.

Arévalo-Martínez, D.L., Haroon, A., Bange, H.W., Erkul, E., Jegen, M., Moosdorf, N., Schneider Von Deimling, J., Berndt, C., Böttcher, M.E., Hoffmann, J., Liebetrau, V., Mallast, U., Massmann, G., Micallef, A., Michael, H.A., Paasche, H., Rabbel, W., Santos, I.R., Scholten, J., Schwalenberg, K., Szymczycha, B., Thomas, A.T., Virtasalo, J.J., Waska, H., Weymer, B.A., 2023. Ideas and perspectives: land-ocean connectivity through groundwater. Biogeosciences 20, 647–662. https://doi.org/10.5194/bg-20-647-2023.

Beck, Aaron J., Rapaglia, John P., Cochran, J. Kirk, Bokuniewicz, Henry J., 2007. Radium mass-balance in Jamaica Bay, NY: Evidence for a Substantial Flux of Submarine Groundwater. https://doi.org/10.1016/j.marchem.2007.03.008.

Beddows, P.A., Smart, P.L., Whitaker, F.F., Smith, S.L., 2007. Decoupled fresh–saline groundwater circulation of a coastal carbonate aquifer: spatial patterns of temperature and specific electrical conductivity. J Hydrol (Amst) 346, 18–32. https://doi.org/10.1016/j.jhydrol.2007.08.013.

Beebe, D., Lowery, B., 2018. Seawater Recirculation Drives Groundwater Nutrient Loading From a Developed Estuary Shoreline With On-site Wastewater Treatment Systems: Mobile Bay, USA. https://doi.org/10.1007/s12665-018-7557-5.

Bejannin, S., van Beek, P., Stieglitz, T.C., Souhaut, M., Tamborski, J.J., 2017. Combining airborne thermal infrared images and radium isotopes to study submarine groundwater discharge along the French Mediterranean coastline. J Hydrol Reg Stud 13, 72–90. https://doi.org/10.1016/j.ejrh.2017.08.001.

Belanger, Thomas V., Price Jr., Thomas L., Heck, Howell H., 2007. Submarine Groundwater Discharge in the Indian River Lagoon, Florida. How Important Is It?.

Bernard, R.J., Mortazavi, B., Wang, L., Ortmann, A.C., MacIntyre, H., Burnett, W.C., 2014. Benthic nutrient fluxes and limited denitrification in a sub-tropical groundwater-influenced coastal lagoon. Mar. Ecol. Prog. Ser. 504, 13–26. https://doi.org/10.3354/meps10783.

Bernard, R.J., Mortazavi, B., Kleinhuizen, A.A., 2015. Dissimilatory nitrate reduction to ammonium (DNRA) seasonally dominates NO3− reduction pathways in an anthropogenically impacted sub-tropical coastal lagoon. Biogeochemistry 125, 47–64. https://doi.org/10.1007/s10533-015-0111-6.

Bokuniewicz, Henry, Taniguchi, Makoto, Ishitoibi, Tomotoshi, Charette, Matthew, Allen, Matthew, Kontar, Evgeny A., 2008. Direct Measurements of Submarine Groundwater Discharge (SGD) over a Fractured Rock Aquifer in Flamengo Bay Brazil. https://doi.org/10.1016/j.ecss.2007.07.047.

Brooks, T.W., Kroeger, K.D., Michael, H.A., York, J.K., 2021. Oxygen-controlled recirculating seepage meter reveals extent of nitrogen transformation in discharging coastal groundwater at the aquifer–estuary interface. Limnol. Oceanogr. 66, 3055–3069. https://doi.org/10.1002/lno.11858.

Bugna, G.C., Chanton, J.P., Cable, J.E., Burnett, W.C., Cable, P.H., 1996. The Importance of Groundwater Discharge to the Methane Budgets of Nearshore and Continental Shelf Waters of the Northeastern Gulf of Mexico. https://doi.org/10.1016/S0016-7037(96)00290-6.

Burnett, W.C., Lambert, M., Dulaiova, H., 2001. Tracing Groundwater Discharge Into the Ocean Via Continuous Radon-222 Measurements.

Burnett, W.C., Cable, J.E., Corbett, D.R., 2003. Radon tracing of submarine groundwater discharge in coastal environments. In: Land and Marine Hydrogeology. Elsevier, pp. 25–43. https://doi.org/10.1016/B978-044451479-0/50015-7.

Burnett, W.C., Aggarwal, P.K., Aureli, A., Bokuniewicz, H.J., Cable, J.E., Charette, M.A., Kontar, E., Krupa, S.L., Kulkarni, K.M., Loveless, A.M., Moore, W.S., Oberdorfer, J.A., Oliveira, J., Ozyurt, N.N., Povinec, P.P., Privitera, A.M.G., Rajar, R., Ramessur, R.T., Scholten, J.C., Stieglitz, T.C., Taniguchi, M., Turner, J.V., 2006. Quantifying submarine groundwater discharge in the coastal zone via multiple methods. Sci. Total Environ. 367, 498–543. https://doi.org/10.1016/j.scitotenv.2006.05.009.

Burnett, William C., Peterson, Richard, Moore, Willard S., de Oliveira, Joselene, 2008. Radon and Radium Isotopes as Tracers of Submarine Groundwater Discharge - Results From the Ubatuba Brazil SGD Assessment Intercomparison. https://doi.org/10.1016/j.ecss.2007.07.027.

Cable, J.E., Martin, J.B., Jaeger, J., 2006. Exonerating Bernoulli? On evaluating the physical and biological processes affecting marine seepage meter measurements. Limnol. Oceanogr. Methods 4, 172–183. https://doi.org/10.4319/lom.2006.4.172.

Canals, M., Ballesteros, E., Amblàs, D., Jordana, E., Pinedo, S., 2021. Cartografia dels fons marins de Sitges: batimetria, sedimentologia i hàbitats bentònics.

Catalunya, G. de, 2010. Llibre verd de l'estat de la zona costanera a Catalunya.

Cerdà-Domènech, M., Rodellas, V., Folch, A., Garcia-orellana, J., 2017. Constraining the temporal variations of Ra isotopes and Rn in the groundwater end-member: implications for derived SGD estimates. Sci. Total Environ. 595, 849–857. https://doi.org/10.1016/j.scitotenv.2017.03.005.

Chaillou, Gwenaelle, Lemay-Borduas, Frederike, Couturier, Mathilde, 2016. Transport and Transformations of Groundwater-borne Carbon Discharging Through a Sandy Beach to a Coastal Ocean. https://doi.org/10.1080/07011784.2015.1111775.

Chanton, J.P., Burnett, W.C., Dulaiova, H., Corbett, D.R., Taniguchi, M., 2003. Seepage Rate Variability in Florida Bay Driven by Atlantic Tidal Height. https://doi.org/10.1023/B:BIOG.0000006168.17717.91.

Chen, X., Cukrov, N.N., Santos, I.R., Rodellas, V., Cukrov, N.N., Du, J., 2020. Karstic submarine groundwater discharge into the Mediterranean: radon-based nutrient fluxes in an anchialine cave and a basin-wide upscaling. Geochim. Cosmochim. Acta 268, 467–484. https://doi.org/10.1016/j.gca.2019.08.019.

Cho, H., Kim, G., 2016. Determining groundwater Ra end-member values for the estimation of the magnitude of submarine groundwater discharge using Ra isotope tracers. Geophys. Res. Lett. 43, 3865–3871. https://doi.org/10.1002/2016GL068805.

CIIRC, 2010. Llibre verd de l'estat de la zona costanera a Catalunya. Centre Internacional D'Investigació Dels Recursos Costaners. Departament de Territori [WWW Document]. URL. https://territori.gencat.cat/ca/01_departament/documentacio/territori-i-urbanisme/ordenacio_territorial/llibre_verd_estat_de_la_zona_costanera/index.html.

Correa, R.E., Tait, D.R., Sanders, C.J., Conrad, S.R., Harrison, D., Tucker, J.P., Reading, M.J., Santos, I.R., 2020. Submarine groundwater discharge and associated nutrient and carbon inputs into Sydney Harbour (Australia). J Hydrol (Amst) 580, 124262. https://doi.org/10.1016/j.jhydrol.2019.124262.

Craddock, Raymond D., Kennedy, Gavin W., Jamieson, Rob C., Keizer, Jonathan, Mohammed, Aaron A., Kurylyk, Barret L., 2022. Assessment of Groundwater Discharge Pathways in a Till-dominated Coastal Aquifer. https://doi.org/10.1016/j.ejrh.2022.101205.

Crusius, J., Koopmans, D., Bratton, J.F., Charette, M.A., Kroeger, K., Henderson, P., Ryckman, L., Halloran, K., Colman, J.A., 2005. Submarine Groundwater Discharge to

a Small Estuary Estimated From Radon and Salinity Measurements and a Box Model. https://doi.org/10.5194/bg-2-141-2005.
Das, K., Debnath, P., Duttagupta, S., Sarkar, S., Agrahari, S., Mukherjee, A., 2020. Implication of submarine groundwater discharge to coastal ecology of the Bay of Bengal. Journal of Earth System Science 129. https://doi.org/10.1007/s12040-019-1317-0.
Day-Lewis, F.D., White, E.A., Johnson, C.D., Lane, J.W., Belaval, M., 2006. Continuous resistivity profiling to delineate submarine groundwater discharge - examples and limitations. Leading Edge (Tulsa, OK) 25, 724–728. https://doi.org/10.1190/1.2210056.
Debbie-Ann, D.S., Gordon-Smith, Greenaway, A.M., 2019. Submarine groundwater discharge and associated nutrient fluxes to Discovery Bay. Jamaica. Estuar Coast Shelf Sci 230, 106431. https://doi.org/10.1016/j.ecss.2019.106431.
Debnath, Palash, Mukherjee, Abhijit, 2016. Quantification of Tidally-influenced Seasonal Groundwater Discharge to the Bay of Bengal by Seepage Meter Study. https://doi.org/10.1016/j.jhydrol.2016.03.010.
Debnath, Palash, Mukherjee, Abhijit, Das, Kousik, 2018. Characterization of tidally influenced seasonal nutrient flux to the Bay of Bengal and its implications on the coastal ecosystem. https://doi.org/10.1002/hyp.11507.
Devol, A.H., 2015. Denitrification, anammox, and N2 production in marine sediments. Ann. Rev. Mar. Sci. 7, 403–423. https://doi.org/10.1146/annurev-marine-010213-135040.
Diego-Feliu, M., Rodellas, V., Alorda-Kleinglass, A., Saaltink, M., Folch, A., Garcia-Orellana, J., 2022. Extreme precipitation events induce high fluxes of groundwater and associated nutrients to coastal ocean. Hydrol. Earth Syst. Sci. 26, 4619–4635. https://doi.org/10.5194/hess-26-4619-2022.
Dulaiova, H., Burnett, W.C., Chanton, J.P., Moore, W.S., Bokuniewicz, H.J., Charette, M. A., Sholkovitz, E., 2006. Assessment of Groundwater Discharges Into West Neck Bay, New York, Via Natural Tracers. https://doi.org/10.1016/j.csr.2006.07.011.
Duque, C., Russoniello, C.J., Rosenberry, D.O., 2020. History and evolution of seepage meters for quantifying flow between groundwater and surface water: part 2 – marine settings and submarine groundwater discharge. Earth Sci Rev 204, 103168. https://doi.org/10.1016/j.earscirev.2020.103168.
Durand, Kalyanie, J.M., 2014. Characterization of the Spatial and Temporal Variations of Submarine Groundwater Discharge Using Electrical Resistivity and Seepage Measurements.
Fear, J.M., Paerl, H.W., Braddy, J.S., 2007. Importance of submarine groundwater discharge as a source of nutrients for the Neuse River Estuary, North Carolina. Estuar. Coasts 30, 1027–1033. https://doi.org/10.1007/BF02841393.
Ford, D., Williams, P., 2007. Karst geomorphology and hydrology. Geogr. J. 157, 87. https://doi.org/10.2307/635167.
Garcia-Orellana, J., Rodellas, V., Tamborski, J., Diego-Feliu, M., van Beek, P., Weinstein, Y., Charette, M., Alorda-Kleinglass, A., Michael, H.A., Stieglitz, T.C., Scholten, J., 2021. Radium isotopes as submarine groundwater discharge (SGD) tracers: review and recommendations. Earth Sci. Rev. 220, 103681. https://doi.org/10.1016/j.earscirev.2021.103681.
Garcia-Solsona, E., Garcia-Orellana, J., Masqué, P., Rodellas, V., Mejías, M., Ballesteros, B.J., Domínguez, J.A., 2010. Groundwater and nutrient discharge through karstic coastal springs (Castelló, Spain). Biogeosciences 7, 2625–2638. https://doi.org/10.5194/bg-7-2625-2010.
Garrison, G.H., Glenn, C.R., McMurtry, G.M., 2003. Measurement of submarine groundwater discharge in Kahana Bay, O'ahu, Hawai'i. Limnol. Oceanogr. 48, 920–928. https://doi.org/10.4319/lo.2003.48.2.0920.
GEM, G. y E.M, 2021. Estudi tècnic sobre l'evolució temporal de la línia de costa i la regeneració de les platges del terme municipal de Sitges.
Goldscheider, N., Chen, Z., Auler, A.S., Bakalowicz, M., Broda, S., Drew, D., Hartmann, J., Jiang, G., Moosdorf, N., Stevanovic, Z., Veni, G., 2020. Global distribution of carbonate rocks and karst water resources. Hydrgeol. J. 28, 1661–1677. https://doi.org/10.1007/s10040-020-02139-5.
Gonneea, M.E., Charette, M.A., 2014. Hydrologic controls on nutrient cycling in an unconfined coastal aquifer. Environ. Sci. Technol. 48, 14178–14185. https://doi.org/10.1021/es503313t.
Gordon-Smith, Debbie-Ann D.S., Greenaway, Anthony M., 2019. Submarine Groundwater Discharge and Associated Nutrient Fluxes to Discovery Bay, Jamaica. https://doi.org/10.1016/j.ecss.2019.106431.
Goyetche, T., Luquot, L., Carrera, J., Martínez-Pérez, L., Folch, A., 2022. Identification and quantification of chemical reactions in a coastal aquifer to assess submarine groundwater discharge composition. Sci. Total Environ. 838, 155978. https://doi.org/10.1016/J.SCITOTENV.2022.155978.
Grünenbaum, N., Ahrens, J., Beck, M., et al., 2020. A Multi-Method Approach for Quantification of In- and Exfiltration Rates From the Subterranean Estuary of a High Energy Beach. https://doi.org/10.3389/feart.2020.571310.
Ibánhez, J.S.P., Leote, C., Rocha, C., 2011. Porewater nitrate profiles in sandy sediments hosting submarine groundwater discharge described by an advection-dispersion-reaction model. Biogeochemistry 103, 159–180. https://doi.org/10.1007/s10533-010-9454-1.
Jiao, L., Wu, J., He, X., Wen, X., Li, Y., Hong, Y., 2018. Significant microbial nitrogen loss from denitrification and anammox in the land-sea interface of low permeable sediments. Int. Biodeter. Biodegr. 135, 80–89. https://doi.org/10.1016/j.ibiod.2018.10.002.
Johannes, R., 1980. The ecological significance of the submarine discharge of groundwater. Mar. Ecol. Prog. Ser. 3, 365–373. https://doi.org/10.3354/meps003365.
Kao, Ruey-Chy, Zavialov, Peter O., Ding, Chung-Feng, 2013. Investigation and Assessment of Submarine Groundwater Discharge of Ping-Tung Nearshore Area in Southwestern Taiwan. https://doi.org/10.1002/ird.1789.
Kobayashi, Shiho, Sugimoto, Ryo, Honda, Hisami, Miyata, Yoji, Tahara, Daisuke, Tominaga, Osamu, Shoji, Jun, Yamada, Makoto, Nakada, Satoshi, Taniguchi, Makoto, 2017. High-resolution Mapping and Time-series Measurements of Rn-222 Concentrations and Biogeochemical Properties Related to Submarine Groundwater Discharge Along the Coast of Obama Bay, a Semi-enclosed Sea in Japan. https://doi.org/10.1186/s40645-017-0124-y.
Kontar, E.A., Ozorovich, Y.R., 2006. Geo-electromagnetic survey of the fresh/salt water interface in the coastal southeastern Sicily. Cont. Shelf Res. 26, 843–851. https://doi.org/10.1016/j.csr.2005.12.012.
Kreuzburg, M., Scholten, J., Hsu, F.H., Liebetrau, V., Sültenfuß, J., Rapaglia, J.P., Schlüter, M., 2023. Submarine groundwater discharge-derived nutrient fluxes in Eckernförde Bay (Western Baltic Sea). Estuaries and Coasts 46, 1190–1207. https://doi.org/10.1007/s12237-023-01202-0.
Kroeger, K.D., Swarzenski, P.W., Greenwood, W.J., Reich, C., 2007. Submarine groundwater discharge to Tampa Bay: nutrient fluxes and biogeochemistry of the coastal aquifer. Mar. Chem. 104, 85–97. https://doi.org/10.1016/j.marchem.2006.10.012.
Lecher, A.L., Mackey, K., 2018. Synthesizing the effects of submarine groundwater discharge on marine biota. Hydrology 5, 60. https://doi.org/10.3390/hydrology5040060.
Lee, D.R., 1977. A device for measuring seepage flux in lakes and estuaries1. Limnol. Oceanogr. 22, 140–147. https://doi.org/10.4319/lo.1977.22.1.0140.
Lee, B., Lee, J., Kim, D., 2018. An Alternative Approach to Conventional Seepage Meters: Buoy-type Seepage Meter. https://doi.org/10.1002/lom3.10246.
Leote, C., Ibánhez, J.S., Rocha, C., 2008. Submarine groundwater discharge as a nitrogen source to the Ria Formosa studied with seepage meters. Biogeochemistry 88, 185–194. https://doi.org/10.1007/s10533-008-9204-9.
Martin, J.B., Cable, J.E., Jaeger, J., Hartl, K., Smith, C.G., 2006. Thermal and chemical evidence for rapid water exchange across the sediment-water interface by bioirrigation in the Indian River Lagoon, Florida. Limnol. Oceanogr. 51, 1332–1341. https://doi.org/10.4319/lo.2006.51.3.1332.
Martin, J.B., Cable, J.E., Smith, C., Roy, M., Cherrier, J., 2007. Magnitudes of submarine groundwater discharge from marine and terrestrial sources: Indian River Lagoon, Florida. Water Resour. Res. 43, 1–15. https://doi.org/10.1029/2006WR005266.
Mejías, M., Ballesteros, B.J., Antón-Pacheco, C., Domínguez, J.A., Garcia-Orellana, J., Garcia-Solsona, E., Masqué, P., 2012. Methodological study of submarine groundwater discharge from a karstic aquifer in the Western Mediterranean Sea. J Hydrol (Amst) 464–465, 27–40. https://doi.org/10.1016/j.jhydrol.2012.06.020.
Michael, H.A., Lubetsky, J.S., Harvey, C.F., 2003. Characterizing Submarine Groundwater Discharge: A Seepage Meter Study in Waquoit Bay, Massachusetts. https://doi.org/10.1029/2002GL016000.
Michael, H.A., Mulligan, A.E., Harvey, C.F., 2005. Seasonal oscillations in water exchange between aquifers and the coastal ocean. Nature 436, 1145–1148. https://doi.org/10.1038/nature03935.
Montiel, D., Dimova, N., Andreo, B., Prieto, J., García-Orellana, J., Rodellas, V., 2018. Assessing submarine groundwater discharge (SGD) and nitrate fluxes in highly heterogeneous coastal karst aquifers: challenges and solutions. J Hydrol (Amst) 557, 222–242. https://doi.org/10.1016/j.jhydrol.2017.12.036.
Moore, W.S., 2010. The effect of submarine groundwater discharge on the ocean. Ann. Rev. Mar. Sci. 2, 59–88. https://doi.org/10.1146/annurev-marine-120308-081019.
Moosdorf, N., Oehler, T., 2017. Societal use of fresh submarine groundwater discharge: an overlooked water resource. Earth Sci Rev 171, 338–348. https://doi.org/10.1016/j.earscirev.2017.06.006.
Mulligan, Ann E., Charette, Matthew A., 2006. Intercomparison of Submarine Groundwater Discharge Estimates From a Sandy Unconfined Aquifer. https://doi.org/10.1016/j.jhydrol.2005.11.056.
Murdoch, L.C., Kelly, S.E., 2003. Factors affecting the performance of conventional seepage meters. Water Resour. Res. 39. https://doi.org/10.1029/2002WR001347.
Mwashote, B.M., Burnett, W.C., Chanton, J., Santos, I.R., Dimova, N., Swarzenski, P.W., 2010. Calibration and Use of Continuous Heat-type Automated Seepage Meters for Submarine Groundwater Discharge Measurements. https://doi.org/10.1016/j.ecss.2009.12.001.
Mwashote, B.M., Murray, M., Burnett, W.C., Chanton, J., Kruse, S., Forde, A., 2013. Submarine Groundwater Discharge in the Sarasota Bay System: Its Assessment and Implications for the Nearshore Coastal Environment. https://doi.org/10.1016/j.csr.2012.12.002.
Nakajima, Toshimi, Sugimoto, Ryo, Tominaga, Osamu, Takeuchi, Masaru, Honda, Hisami, Shoji, Jun, Taniguchi, Makoto, 2018. Fresh and Recirculated Submarine Groundwater Discharge Evaluated by Geochemical Tracers and a Seepage Meter at Two Sites in the Seto Inland Sea, Japan. https://doi.org/10.3390/hydrology5040061.
Null, Kimberly A., Corbett, D. Reide, DeMaster, David J., Burkholder, JoAnn M., Thomas, Carrie J., Reed, Robert E., 2011. Porewater Advection of Ammonium Into the Neuse River Estuary, North Carolina, USA. https://doi.org/10.1016/j.ecss.2011.09.016.
Null, K.A., Knee, K.L., Crook, E.D., de Sieyes, N.R., Rebolledo-Vieyra, M., Hernández-Terrones, L., Paytan, A., 2014. Composition and fluxes of submarine groundwater along the Caribbean coast of the Yucatan Peninsula. Cont. Shelf Res. 77, 38–50. https://doi.org/10.1016/j.csr.2014.01.011.
O'Connor, A.E., Luek, J.L., McIntosh, H., Beck, A.J., 2015. Geochemistry of redox-sensitive trace elements in a shallow subterranean estuary. Mar. Chem. 172, 70–81. https://doi.org/10.1016/j.marchem.2015.03.001.
Paepen, M., Hanssens, D., De Smedt, P., Walraevens, K., Hermans, T., 2020. Combining resistivity and frequency domain electromagnetic methods to investigate submarine groundwater discharge in the littoral zone. Hydrol. Earth Syst. Sci. 24, 3539–3555. https://doi.org/10.5194/hess-24-3539-2020.

Pain, A.J., Martin, J.B., Young, C.R., Huang, L., Valle-Levinson, A., 2019. Organic matter quantity and quality across salinity gradients in conduit- vs. diffuse flow-dominated subterranean estuaries. Limnol. Oceanogr. 64, 1386–1402. https://doi.org/10.1002/lno.11122.

Pain, A.J., Martin, J.B., Young, C.R., 2021. Biogeochemical and hydrological drivers of heterogeneous nutrient exports from subterranean estuaries. Front. Mar. Sci. 8, 1–15. https://doi.org/10.3389/fmars.2021.699916.

Pavlidou, A., Papadopoulos, V.P., Hatzianestis, I., Simboura, N., Patiris, D., Tsabaris, C., 2014. Chemical inputs from a karstic submarine groundwater discharge (SGD) into an oligotrophic Mediterranean coastal area. Sci. Total Environ. 488–489, 1–13. https://doi.org/10.1016/j.scitotenv.2014.04.056.

Peterson, Richard N., Burnett, William C., Taniguchi, Makoto, Chen, Jianyao, Santos, Isaac R., Ishitobi, Tomotoshi, 2008. Radon and Radium Isotope Assessment of Submarine Groundwater Discharge in the Yellow River Delta, China. https://doi.org/10.1029/2008JC004776.

Povinec, P., Bokuniewicz, H., Burnett, W., et al., 2008. Isotope Tracing of Submarine Groundwater Discharge Offshore Ubatuba, Brazil: Results of the IAEA-UNESCO SGD Project. https://doi.org/10.1016/j.jenvrad.2008.06.010.

Povinec, P.P., Burnett, W.C., Beck, A., Bokuniewicz, H., Charette, M., Gonneea, M.E., Groening, M., Ishitobi, T., Kontar, E., Liong Wee Kwong, L., Marie, D.E.P., Moore, W. S., Oberdorfer, J.A., Peterson, R., Ramessur, R., Rapaglia, J.P., Stieglitz, T.C., Top, Z., 2012. Isotopic, geophysical and biogeochemical investigation of submarine groundwater discharge: IAEA-UNESCO intercomparison exercise at Mauritius Island. J. Environ. Radioact. 104, 24–45. https://doi.org/10.1016/j.jenvrad.2011.09.009.

Prakash, R., Srinivasamoorthy, K., Gopinath, S., Saravanan, K., 2018. Measurement of submarine groundwater discharge using diverse methods in Coleroon Estuary, Tamil Nadu, India. Appl Water Sci 8, 1–11. https://doi.org/10.1007/s13201-018-0659-0.

Puertos del Estado, 2023. Prediccion de oleaje, nivel del mar; Boyas y mareografos | puertos.es [WWW Document]. URL. https://www.puertos.es/en-us/oceanografia/Pages/portus.aspx.

Puertos del Estado, 2024. Prediccion de oleaje, nivel del mar; Boyas y mareografos | puertos.es [WWW Document]. URL. https://www.puertos.es/es-es/oceanografia/Paginas/portus.aspx.

Rapaglia, J.P., 2005. Submarine groundwater discharge into Venice Lagoon, Italy. Estuaries 28, 705–713. https://doi.org/10.1007/BF02732909.

Rapaglia, J., Di Sipio, E., Bokuniewicz, H., et al., 2010. Groundwater Connections Under a Barrier Beach: A Case Study in the Venice Lagoon. https://doi.org/10.1016/j.csr.2009.10.001.

Remy, N., Boucher, A., Wu, J., 2009. Applied Geostatistics with SGeMS. Applied Geostatistics with SGeMS. https://doi.org/10.1017/cbo9781139150019.

Richardson, C.M., Davis, K.L., Ruiz-González, C., Guimond, J.A., Michael, H.A., Paldor, A., Moosdorf, N., Paytan, A., 2024. The impacts of climate change on coastal groundwater. Nat Rev Earth Environ. https://doi.org/10.1038/s43017-023-00500-2.

Rigaud, S., Radakovitch, O., Couture, R.M., Deflandre, B., Cossa, D., Garnier, C., Garnier, J.M., 2013. Mobility and fluxes of trace elements and nutrients at the sediment-water interface of a lagoon under contrasting water column oxygenation conditions. Appl. Geochem. 31, 35–51. https://doi.org/10.1016/j.apgeochem.2012.12.003.

Robinson, C.E., Xin, P., Santos, I.R., Charette, M.A., Li, L., Barry, D.A., 2018. Groundwater dynamics in subterranean estuaries of coastal unconfined aquifers: controls on submarine groundwater discharge and chemical inputs to the ocean. Adv. Water Resour. 115, 315–331. https://doi.org/10.1016/j.advwatres.2017.10.041.

Rocha, C., Ibanhez, J., Leote, C., 2009. Benthic Nitrate Biogeochemistry Affected by Tidal Modulation of Submarine Groundwater Discharge (SGD) Through a Sandy Beach Face, Ria Formosa, Southwestern Iberia. https://doi.org/10.1016/j.marchem.2009.06.003.

Rodellas, V., Garcia-Orellana, J., Masqué, P., Feldman, M., Weinstein, Y., 2015. Submarine groundwater discharge as a major source of nutrients to the Mediterranean Sea. Proc. Natl. Acad. Sci. 112, 3926–3930. https://doi.org/10.1073/pnas.1419049112.

Rodellas, V., Stieglitz, T.C., Andrisoa, A., Cook, P.G., Raimbault, P., Tamborski, J.J., van Beek, P., Radakovitch, O., 2018. Groundwater-driven nutrient inputs to coastal lagoons: the relevance of lagoon water recirculation as a conveyor of dissolved nutrients. Sci. Total Environ. 642, 764–780. https://doi.org/10.1016/j.scitotenv.2018.06.095.

Rodellas, V., Stieglitz, T.C., Tamborski, J.J., Beek, P., Andrisoa, A., Cook, P.G., 2021. Conceptual uncertainties in groundwater and porewater fluxes estimated by radon and radium mass balances. Limnol. Oceanogr. 66, 1237–1255. https://doi.org/10.1002/lno.11678.

Roy, M., Rouxel, O., Martin, J.B., Cable, J.E., 2012. Iron isotope fractionation in a sulfide-bearing subterranean estuary and its potential influence on oceanic Fe isotope flux. Chem. Geol. 300–301, 133–142. https://doi.org/10.1016/j.chemgeo.2012.01.022.

Roy, M., Martin, J.B., Cable, J.E., Smith, C.G., 2013. Variations of iron flux and organic carbon remineralization in a subterranean estuary caused by inter-annual variations in recharge. Geochim. Cosmochim. Acta 103, 301–315. https://doi.org/10.1016/j.gca.2012.10.055.

Russoniello, C., Fernandez, C., Bratton, J., et al., 2013. Geologic Effects on Groundwater Salinity and Discharge Into an Estuary. https://doi.org/10.1016/j.jhydrol.2013.05.049.

Russoniello, C.J., Konikow, L.F., Kroeger, K.D., Fernandez, C., Andres, A.S., Michael, H.A., 2016. Hydrogeologic controls on groundwater discharge and nitrogen loads in a coastal watershed. J Hydrol (Amst) 538, 783–793. https://doi.org/10.1016/j.jhydrol.2016.05.013.

Santos, Isaac R., Burnett, William C., Chanton, Jeffrey, Dimova, Natasha, Peterson, Richard N., 2009. Land or Ocean?: Assessing the Driving Forces of Submarine Groundwater Discharge at a Coastal Site in the Gulf of Mexico. https://doi.org/10.1029/2008JC005038.

Santos, I.R., Eyre, B.D., Huettel, M., 2012. The driving forces of porewater and groundwater flow in permeable coastal sediments: a review. Estuar. Coast. Shelf Sci. 98, 1–15. https://doi.org/10.1016/j.ecss.2011.10.024.

Santos, I.R., Chen, X., Lecher, A.L., Sawyer, A.H., Moosdorf, N., Rodellas, V., Tamborski, J.J., Cho, H., Dimova, N., Sugimoto, R., Bonaglia, S., Li, H., Hajati, M.-C., Li, L., 2021. Submarine groundwater discharge impacts on coastal nutrient biogeochemistry. Nat Rev Earth Environ 2, 307–323. https://doi.org/10.1038/s43017-021-00152-0.

Sawyer, A.H., Lazareva, O., Kroeger, K.D., Crespo, K., Chan, C.S., Stieglitz, T.C., Michael, H.A., 2014. Stratigraphic controls on fluid and solute fluxes across the sediment-water interface of an estuary. Limnol. Oceanogr. 59, 997–1010. https://doi.org/10.4319/lo.2014.59.3.0997.

Schlueter, Michael, Maier, Philipp, 2021. Submarine Groundwater Discharge From Sediments and Sand Boils Quantified by the Mean Residence Time of a Tracer Injection. https://doi.org/10.3389/feart.2021.710000.

Schlüter, M., Sauter, E., Hansen, H.-P., Suess, E., 2000. Seasonal variations of bioirrigation in coastal sediments: modelling of field data. Geochim. Cosmochim. Acta 64, 821–834. https://doi.org/10.1016/S0016-7037(99)00375-0.

Shinn, E.A., Reich, C.D., Hickey, T.D., 2002. Seepage meters and Bernoulli's revenge. Estuaries 25, 126–132. https://doi.org/10.1007/BF02696056.

Sholkovitz, Edward, Herbold, Craig, Charette, Matthew, 2003. An Automated Dye-dilution Based Seepage Meter for the Time-series Measurement of Submarine Groundwater Discharge. https://doi.org/10.4319/lom.2003.1.16.

Slomp, C.P., Van Cappellen, P., 2004. Nutrient inputs to the coastal ocean through submarine groundwater discharge: controls and potential impact. J Hydrol (Amst) 295, 64–86. https://doi.org/10.1016/j.jhydrol.2004.02.018.

SMC, 2023. Climatologies comarcals - Servei Meteorològic de Catalunya | Meteocat [WWW Document]. URL. https://www.meteo.cat/wpweb/climatologia/el-clima/climatologies-comarcals/ (accessed 11.29.23).

Smith, C.F., Chadwick, D.B., Paulsen, R.J., Groves, J.G., 2003. Development and Deployment of an Ultrasonic Groundwater Seepage Meter: A Reliable Way to Measure Groundwater Seepage. https://doi.org/10.1109/OCEANS.2003.178537.

Spiteri, C., Slomp, C.P., Charette, M.A., Tuncay, K., Meile, C., 2008a. Flow and nutrient dynamics in a subterranean estuary (Waquoit Bay, MA, USA): field data and reactive transport modeling. Geochim. Cosmochim. Acta 72, 3398–3412. https://doi.org/10.1016/j.gca.2008.04.027.

Spiteri, C., Slomp, C.P., Tuncay, K., Meile, C., 2008b. Modeling biogeochemical processes in subterranean estuaries: effect of flow dynamics and redox conditions on submarine groundwater discharge of nutrients. Water Resour. Res. 44, 1–18. https://doi.org/10.1029/2007WR006071.

Stieglitz, T., Rapaglia, J., Krupa, S., 2007. An Effect of Pier Pilings on Nearshore Submarine Groundwater Discharge From a (Partially) Confined Aquifer. https://doi.org/10.1007/bf03036520.

Stieglitz, T., Taniguchi, M., Neylon, S., 2008. Spatial variability of submarine groundwater discharge, Ubatuba, Brazil. Estuar. Coast. Shelf Sci. 76, 493–500. https://doi.org/10.1016/j.ecss.2007.07.038.

Stieglitz, T.C., Rapaglia, J.P., Bokuniewicz, H., 2008a. Estimation of submarine groundwater discharge from bulk ground electrical conductivity measurements. J Geophys Res Oceans 113. https://doi.org/10.1029/2007JC004499.

Stieglitz, T.C., Rapaglia, J.P., Bokuniewicz, H.J., 2008b. Estimation of submarine groundwater discharge from bulk ground electrical conductivity measurements. J Geophys Res Oceans 113, 1–15. https://doi.org/10.1029/2007JC004499.

Swarzenski, P.W., Izbicki, J.A., 2009. Coastal groundwater dynamics off Santa Barbara, California: combining geochemical tracers, electromagnetic seepmeters, and electrical resistivity. Estuar. Coast. Shelf Sci. 83, 77–89. https://doi.org/10.1016/j.ecss.2009.03.027.

Swarzenski, P.W., Burnett, W.C., Greenwood, W.J., Herut, B., Peterson, R., Dimova, N., Shalem, Y., Yechieli, Y., Weinstein, Y., 2006a. Combined time-series resistivity and geochemical tracer techniques to examine submarine groundwater discharge at Dor Beach, Israel. Geophys. Res. Lett. 33, 1–6. https://doi.org/10.1029/2006GL028282.

Swarzenski, Peter W., Orem, William H., McPherson, Benjamin F., Baskaran, Mark, Wan, Yongshan, 2006b. Biogeochemical transport in the Loxahatchee River estuary, Florida: The Role of Submarine Groundwater Discharge. https://doi.org/10.1016/j.marchem.2006.03.007.

Swarzenski, P.W., Simonds, F.W., Paulson, A.J., Kruse, S., Reich, C., 2007. Geochemical and geophysical examination of submarine groundwater discharge and associated nutrient loading estimates into lynch cove, Hood Canal, WA. Environ. Sci. Technol. 41, 7022–7029. https://doi.org/10.1021/es070881a.

Szymczycha, B., Vogler, S., Pempkowiak, J., 2012. Nutrient fluxes via submarine groundwater discharge to the Bay of Puck, southern Baltic Sea. Sci. Total Environ. 438, 86–93. https://doi.org/10.1016/j.scitotenv.2012.08.058.

Szymczycha, B., Kroeger, K., Pempkowiak, J., 2016. Significance of groundwater discharge Along the Coast of Poland as a Source of Dissolved Metals to the Southern Baltic Sea. https://doi.org/10.1016/j.marpolbul.2016.06.008.

Tait, D.R., Santos, I.R., Erler, D.V., Befus, K.M., Cardenas, M.B., Eyre, B.D., 2013. Estimating submarine groundwater discharge in a South Pacific coral reef lagoon using different radioisotope and geophysical approaches. Mar. Chem. 156, 49–60. https://doi.org/10.1016/j.marchem.2013.03.004.

Tamborski, J.J., Cochran, J.K., Bokuniewicz, H.J., 2017. Submarine Groundwater Discharge Driven Nitrogen Fluxes to Long Island Sound, NY: Terrestrial vs. Marine Sources. https://doi.org/10.1016/j.gca.2017.09.003.

Tamborski, J.J., van Beek, P., Conan, P., Pujo-Pay, M., Odobel, C., Ghiglione, J.F., Seidel, J.L., Arfib, B., Diego-Feliu, M., Garcia-Orellana, J., Szafran, A., Souhaut, M., 2020. Submarine karstic springs as a source of nutrients and bioactive trace metals for the oligotrophic Northwest Mediterranean Sea. Sci. Total Environ. 732, 1–14. https://doi.org/10.1016/j.scitotenv.2020.139106.

Taniguchi, M., 2002. Tidal Effects on Submarine Groundwater Discharge Into the Ocean. https://doi.org/10.1029/2002GL014987.

Taniguchi, M., 2006. Submarine Groundwater Discharge Measured by Seepage Meters in Sicilian Coastal Waters. https://doi.org/10.1016/j.csr.2005.12.002.

Taniguchi, M., Iwakawa, H., 2004. Submarine Groundwater Discharge in Osaka Bay, Japan. https://doi.org/10.1007/s10201-003-0112-3.

Taniguchi, M., Burnett, W.C., Cable, J.E., Turner, J.V., 2002. Investigation of submarine groundwater discharge. Hydrol. Process. 16, 2115–2129. https://doi.org/10.1002/hyp.1145.

Taniguchi, M., Burnett, W.C., Smith, C.F., Paulsen, R.J., O'Rourke, D., Krupa, S.L., Christoff, J.L., 2003. Spatial and temporal distributions of submarine groundwater discharge rates obtained from various types of seepage meters at a site in the Northeastern Gulf of Mexico. Biogeochemistry 66, 35–53. https://doi.org/10.1023/B:BIOG.0000006090.25949.8d.

Taniguchi, M., Ishitobi, T., Shimada, J., Takamoto, N., 2006a. Evaluations of spatial distribution of submarine groundwater discharge. Geophys. Res. Lett. 33, 2–5. https://doi.org/10.1029/2005GL025288.

Taniguchi, M., Ishitobi, T., Shimada, J., 2006b. Dynamics of submarine groundwater discharge and freshwater-seawater interface. J Geophys Res Oceans 111, 1–9. https://doi.org/10.1029/2005JC002924.

Taniguchi, M., Ishitobi, T., William Burnett, C., Shimada, J., 2007. Comprehensive evaluation of the groundwater-seawater interface and submarine groundwater discharge. IAHS-AISH Publication 86–92.

Taniguchi, M., Stieglitz, T.C., Ishitobi, T., 2008a. Temporal variability of water quality of submarine groundwater discharge in Ubatuba, Brazil. Estuar. Coast. Shelf Sci. 76, 484–492. https://doi.org/10.1016/j.ecss.2007.07.019.

Taniguchi, Makoto, Burnett, William C., Dulaiova, Henrieta, Siringan, Fernando, Foronda, Joseph, Wattayakorn, Gullaya, Rungsupa, Sompop, Kontar, Evgueni A., Ishitobi, Tomotoshi, 2008b. Groundwater Discharge as an Important Land-sea Pathway Into Manila Bay, Philippines. https://doi.org/10.2112/06-0636.1.

Taniguchi, Makoto, Ishitobi, Tomotoshi, Chen, Jianyao, Onodera, Shin-ichi, Miyaoka, Kunihide, Burnett, William C., Peterson, Richard, Liu, Guanqun, Fukushima, Yoshihiro, 2008c. Submarine Groundwater Discharge From the Yellow River Delta to the Bohai Sea, China. https://doi.org/10.1029/2007JC004498.

Taniguchi, Makoto, Ono, Masahiko, Takahashi, Masahiro, 2014. Multi-scale Evaluations of Submarine Groundwater Discharge.

Taniguchi, M., Dulai, H., Burnett, K.M., Santos, I.R., Sugimoto, R., Stieglitz, T.C., Kim, G., Moosdorf, N., Burnett, W.C., 2019. Submarine groundwater discharge: updates on its measurement techniques, geophysical drivers, magnitudes, and effects. Front. Environ. Sci. 7, 1–26. https://doi.org/10.3389/fenvs.2019.00141.

Tirado-Conde, Joel, Engesgaard, Peter, Karan, Sachin, Mueller, Sascha, Duque, Carlos, 2019. Evaluation of Temperature Profiling and Seepage Meter Methods for Quantifying Submarine Groundwater Discharge to Coastal Lagoons: Impacts of Saltwater Intrusion and the Associated Thermal Regime. https://doi.org/10.3390/w11081648.

Tovar-Sánchez, A., Basterretxea, G., Rodellas, V., Sánchez-Quiles, D., García-Orellana, J., Masqué, P., Jordi, A., López, J.M., Garcia-Solsona, E., 2014. Contribution of groundwater discharge to the coastal dissolved nutrients and trace metal concentrations in Majorca Island: karstic vs detrital systems. Environ. Sci. Technol. 48. https://doi.org/10.1021/es502958t.

Tur-Piedra, J., Ledo, J., Diego-Feliu, M., Queralt, P., Marcuello, A., Rodellas, V., Folch, A., 2024. Spatial and seasonal fluctuations in fresh submarine groundwater discharge revealed by marine continuous resistivity profiling. Sci. Rep. 14, 24854. https://doi.org/10.1038/s41598-024-75984-z.

Turner, R.R., Kopec, A.D., Charette, M.A., Henderson, P.B., 2018. Current and Historical Rates of Input of Mercury to the Penobscot River, Maine, From a Chlor-alkali Plant. https://doi.org/10.1016/j.scitotenv.2018.05.090.

Uddameri, Venkatesh, Singaraju, Sreeram, Hernandez, E. Annette, 2014. Temporal Variability of Freshwater and Pore Water Recirculation Components of Submarine Groundwater Discharges at Baffin Bay, Texas. https://doi.org/10.1007/s12665-013-2902-1.

Uemura, Takeshi, Taniguchi, Makoto, Shibuya, Kazuo, 2011. Submarine Groundwater Discharge in Lutzow-Holm Bay, Antarctica. https://doi.org/10.1029/2010GL046394.

Vanek, V., Lee, D.R., 1991. Mapping Submarine Groundwater Discharge Areas - An Example From Laholm Bay, Southwest Sweden.

Vanek, V., 1991. Mapping submarine groundwater discharge areas - an example from Laholm Bay, southwest Sweden. Limnol. Oceanogr. 1250–1262.

W. Brooks, T., D. Kroeger, K., A. Michael, H., K. York, J., 2021. Oxygen-controlled recirculating seepage meter reveals extent of nitrogen transformation in discharging coastal groundwater at the aquifer–estuary interface. Limnol. Oceanogr. 66, 3055–3069. https://doi.org/10.1002/lno.11858.

Ward, A.S., Gooseff, M.N., Singha, K., 2010. Characterizing hyporheic transport processes - interpretation of electrical geophysical data in coupled stream-hyporheic zone systems during solute tracer studies. Adv. Water Resour. 33, 1320–1330. https://doi.org/10.1016/j.advwatres.2010.05.008.

Weinstein, Y., Yechieli, Y., Shalem, Y., Burnett, W.C., Swarzenski, P.W., Herut, B., 2011. What is the role of fresh groundwater and recirculated seawater in conveying nutrients to the coastal ocean? Environ. Sci. Technol. 45, 5195–5200. https://doi.org/10.1021/es104394r.

Wilson, S.J., Moody, A., McKenzie, T., Cardenas, M.B., Luijendijk, E., Sawyer, A.H., Wilson, A.M., Xu, B., Knee, K.L., Cho, H., Weinstein, Y., Paytan, A., Moosdorf, N., Chen, C.T.A., Beck, M., Lopez, C., Murgulet, D., Kim, G., Charette, M.A., Waska, H., Ibánhez, J.S.P., Chaillou, G., Oehler, T., Onodera, S. ichi, Saito, M., Rodellas, V., Dimova, N., Montiel, D., Dulai, H., Richardson, C.M., Du, J., Petermann, E., Chen, X., Davis, K.L., Lamontagne, S., Sugimoto, R., Wang, G., Li, H., Torres, A.I., Demir, C., Bristol, E., Connolly, C.T., McClelland, J.W., Silva, B.J., Tait, D.R., Kumar, B.S.K., Viswanadham, R., Sarma, V.V.S.S., Silva-Filho, E., Shiller, A., Lecher, A.L., Tamborski, J.J., Bokuniewicz, H., Rocha, C., Reckhardt, A., Böttcher, M.E., Jiang, S., Stieglitz, T.C., Gbewezoun, H.G.V., Charbonnier, C., Anschutz, P., Hernández-Terrones, L.M., Babu, S., Szymczycha, B., Sadat-Noori, M., Niencheski, F., Null, K.A., Tobias, C., Song, B., Anderson, I.C., Santos, I.R., 2024. Global subterranean estuaries modify groundwater nutrient loading to the ocean. Limnol Oceanogr Lett 411–422. https://doi.org/10.1002/lol2.10390.

Windom, H.L., Niencheski, F., 2003. Biogeochemical processes in a freshwater–seawater mixing zone in permeable sediments along the coast of Southern Brazil. Mar. Chem. 83, 121–130. https://doi.org/10.1016/S0304-4203(03)00106-3.

Wong, W.W., Applegate, A., Poh, S.C., Cook, P.L.M., 2020. Biogeochemical attenuation of nitrate in a sandy subterranean estuary: insights from two stable isotope approaches. Limnol. Oceanogr. 65, 3098–3113. https://doi.org/10.1002/lno.11576.

Wu, J., Hong, Y., Wilson, S.J., Song, B., 2021. Microbial nitrogen loss by coupled nitrification to denitrification and anammox in a permeable subterranean estuary at Gloucester Point, Virginia. Mar Pollut Bull 168, 112440. https://doi.org/10.1016/j.marpolbul.2021.112440.

Zhang, X., Sawyer, A.H., Singha, K., 2023. A numerical exploration of hyporheic zone solute transport behavior estimated from electrical resistivity inversions. J Hydrol (Amst) 621, 129577. https://doi.org/10.1016/j.jhydrol.2023.129577.